Cell Metabolism

Article

Excess pancreatic elastase alters acinar-β cell communication by impairing the mechano-signaling and the PAR2 pathways

Graphical abstract

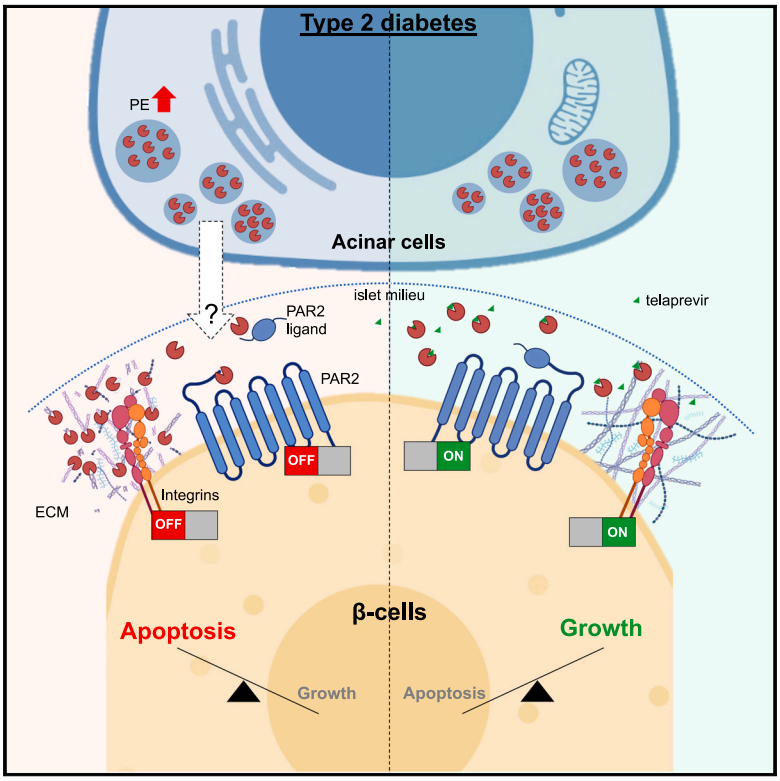

Highlights

- CELA3B, an exocrine gene, is upregulated in acinar cells of patients with T2D
- CELA3B protein deposits in islet milieu and compromises β cell homeostasis in T2D
- Telaprevir, a PE inhibitor, improves viability and function of human β cells
- PE affects β cell homeostasis by impairing mechano-signaling and PAR2 pathways

Authors

Giorgio Basile, Amedeo Vetere, Jiang Hu, ..., Amit Choudhary, Bridget K. Wagner, Rohit N. Kulkarni

Correspondence

rohit.kulkarni@joslin.harvard.edu

In brief

Basile et al. observed CELA3B genes upregulated in acinar cells linked to augmented CELA3B protein within islet milieu of T2D patients, resulting in reduced β cell homeostasis secondary to impairment of two signaling hubs: mechano-signaling and PAR2 pathways. PE inhibitors rescue β cell homeostasis and point to anti-PE therapies in T2D.

Basile et al., 2023, Cell Metabolism *35*, 1–19
July 11, 2023
https://doi.org/10.1016/j.cmet.2023.05.007

CellPress

Please cite this article in press as: Basile et al., Excess pancreatic elastase alters acinar-β cell communication by impairing the mechano-signaling and the PAR2 pathways, Cell Metabolism (2023), https://doi.org/10.1016/j.cmet.2023.05.007

Cell Metabolism

CellPress

Article

Excess pancreatic elastase alters acinar-β cell communication by impairing the mechano-signaling and the PAR2 pathways

Giorgio Basile,[1] Amedeo Vetere,[2] Jiang Hu,[1] Oluwaseun Ijaduola,[1] Yi Zhang,[1] Ka-Cheuk Liu,[3] Amira M. Eltony,[4] Dario F. De Jesus,[1] Kazuki Fukuda,[1] Grace Doherty,[1] Colin A. Leech,[5] Oleg G. Chepurny,[5] George G. Holz,[5,6] Seok-Hyun Yun,[4,7] Olov Andersson,[3] Amit Choudhary,[2] Bridget K. Wagner,[2] and Rohit N. Kulkarni[1,8,*]

[1]Section on Islet Cell and Regenerative Biology, Joslin Diabetes Center, Department of Medicine, Beth Israel Deaconess Medical Center, Harvard Medical School, Harvard Stem Cell Institute, Boston, MA 02215, USA

[2]Chemical Biology and Therapeutics Science Program, Broad Institute of Harvard and MIT, Cambridge, MA 02142, USA

[3]Department of Cell and Molecular Biology, Karolinska Institutet, Stockholm 171 77, Sweden

[4]Harvard Medical School and Wellman Center for Photomedicine, Massachusetts General Hospital, Boston, MA 02114, USA

[5]Department of Medicine, State University of New York (SUNY) Upstate Medical University, Syracuse, NY 13210, USA

[6]Department of Pharmacology, State University of New York (SUNY) Upstate Medical University, Syracuse, NY 13210, USA

[7]Harvard-MIT Division of Health Sciences and Technology, Cambridge, MA 02139, USA

[8]Lead contact

*Correspondence: rohit.kulkarni@joslin.harvard.edu

https://doi.org/10.1016/j.cmet.2023.05.007

SUMMARY

Type 1 (T1D) or type 2 diabetes (T2D) are caused by a deficit of functional insulin-producing β cells. Thus, the identification of β cell trophic agents could allow the development of therapeutic strategies to counteract diabetes. The discovery of SerpinB1, an elastase inhibitor that promotes human β cell growth, prompted us to hypothesize that pancreatic elastase (PE) regulates β cell viability. Here, we report that PE is up-regulated in acinar cells and in islets from T2D patients, and negatively impacts β cell viability. Using high-throughput screening assays, we identified telaprevir as a potent PE inhibitor that can increase human and rodent β cell viability *in vitro* and *in vivo* and improve glucose tolerance in insulin-resistant mice. Phospho-antibody microarrays and single-cell RNA sequencing analysis identified PAR2 and mechano-signaling pathways as potential mediators of PE. Taken together, our work highlights PE as a potential regulator of acinar-β cell crosstalk that acts to limit β cell viability, leading to T2D.

INTRODUCTION

Type 1 (T1D) and type 2 diabetes (T2D) are characterized by a progressive loss of functional β cell mass.[1,2] Approaches aimed at increasing functional β cell numbers to counteract diabetes in patients include delivery of stem-cell-derived insulin-producing cells,[3,4] stimulating neogenesis from ductal pancreatic progenitors,[5,6] inducing proliferation of pre-existing β cells, or counteracting β cell apoptosis.[7] Multiple small molecules, including inhibitors of dual-specificity tyrosine phosphorylation-regulated kinase 1A (DYRK1A),[8,9] glycogen synthase kinase 3 beta (GSK3β),[10] or transforming growth factor beta (TGF-β) pathways,[11] and endogenous factors including osteoprotegerin[12] and leukemia inhibitory factor (LIF),[13] have been shown to induce β cell proliferation. Our lab identified SerpinB1, derived from the liver and elevated in insulin-resistant states, as an endogenous protease inhibitor that promotes human β cell proliferation.[14] Among the proteases inhibited by SerpinB1, including elastases, cathepsin G, and proteinase 3, we focused on pancreatic elastase (PE) as a primary target of its actions on β cells for several reasons. First, the role of SerpinB1 as a β cell trophic factor is directly related to its ability to inhibit elastase activity.[14] Second, sivelestat and GW311616A, known elastase inhibitors, are both able to enhance human β cell proliferation.[14] Third, PE is relevant in the context of diabetes[15,16] and its fecal levels are altered in patients with T2D, who also exhibit reduced functional β cell mass.[2,17] It is worth noting that polymorphisms in the chymotrypsin-like elastase (CELA) *2A* (*CELA2A*), *CELA3B* (two of the PE genes), and *SERPINB1* loci are associated with multigenerational diabetes in human families.[14,18,19] Finally, elastase regulates the viability of different cell types, either by impacting the integrin/focal adhesion pathway to modulate ECM remodeling,[20] collectively termed mechano-signaling, or the protease-activated receptor (PAR) pathway.[21] The latter observation gains significance because PAR2 and PAR3 are expressed in β cells, and have been linked to insulin secretion.[22,23] However, the overall integration of mechano-signaling and PARs signaling in the context of the deleterious effects of PE on β cells and exocrine-endocrine crosstalk has not been explored in detail.

Please cite this article in press as: Basile et al., Excess pancreatic elastase alters acinar-β cell communication by impairing the mechano-signaling and the PAR2 pathways, Cell Metabolism (2023), https://doi.org/10.1016/j.cmet.2023.05.007

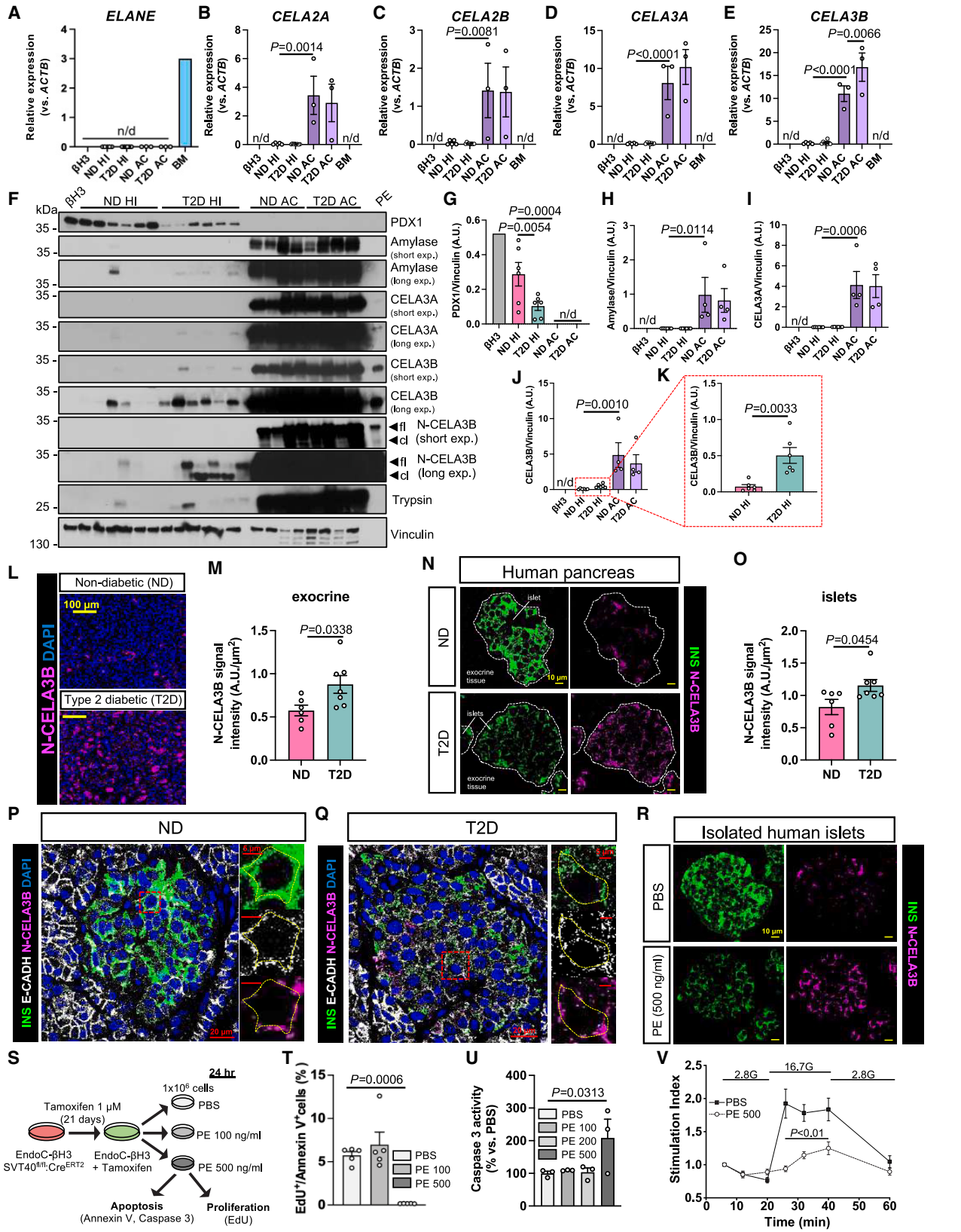

(legend on next page)

Please cite this article in press as: Basile et al., Excess pancreatic elastase alters acinar-β cell communication by impairing the mechano-signaling and the PAR2 pathways, Cell Metabolism (2023), https://doi.org/10.1016/j.cmet.2023.05.007

Here, we report that PE levels are elevated in exocrine and endocrine pancreas in T2D. We also show that the detrimental effects of PE on human β cell viability due to impairment of the mechano-signaling and PAR2 pathways are reversed by a potent and specific PE inhibitor, telaprevir. Taken together, our studies identify PE as a regulator of the crosstalk between acinar and β cells and highlight PE inhibitors as potential therapeutic candidates to increase β cell numbers in patients with diabetes.

RESULTS

PE is increased in human acinar cells and islets of patients with T2D

We first examined the expression levels of elastases and other proteases inhibited by SerpinB1 in isolated human islets (HI) and acinar cells (ACs) from non-diabetic (ND) and T2D donors. The EndoC-βH3 (βH3) cell line[24] was used to represent human β cells. This analysis revealed that while neutrophil proteases, including elastase (*ELANE*) (Figure 1A) and cathepsin G (*CTSG*) (Figure S1A), were virtually absent in pancreatic samples, the *CELA* genes coding for PE proteins (i.e., *CELA2A*, *CELA2B*, *CELA3A*, and *CELA3B*) were expressed exclusively in human ACs (Figures 1B–1E) and virtually absent in either pure β cells or human islets. Among these, *CELA3B* transcripts were significantly up-regulated in ACs from donors with T2D compared with ND samples (Figure 1E). The purity of the human islet and AC preparations were confirmed by exclusive expression of amylase α-2A (*AMY2A*), an AC marker, and pancreatic and duodenal homeobox 1 (*PDX1*), an endocrine cell marker gene (Figures S1B and S1C). As expected, the expression of the latter was lower in T2D islets compared with ND samples[25] (Figure S1C). Additionally, ductal cell genes, such as cytokeratin 19 (*KRT19*) and mucin 1 (*MUC1*), were expressed at minimal levels in the AC preparations compared with their expression in primary human ductal cells (Figures S1D and S1E), indicating null spontaneous differentiation into the ductal lineage.

Then, we evaluated protein levels of CELA3B and its paralog CELA3A by western blotting, including a human PE preparation, containing all forms of CELA proteins, as positive control. Because CELA3B is produced as a proenzyme (inactive, hereinafter referred to as the full-length form or CELA3B) in ACs, and it is cleaved by trypsin at the Arg28 residue in the N-terminal domain and converted into the active enzyme (hereinafter referred to as the cleaved form or N-CELA3B),[19] we explored the expression of both forms of CELA3B in pancreatic samples using two distinguishing antibodies: one with higher affinity for the full-length form (aa 1–270) and one specific for the N-terminal domain of the cleaved form (aa 29–270). The affinity of the two antibodies was tested by using increasing amounts of PE, which contains the full-length form of CELA3B, and of a recombinant human CELA3B protein corresponding to the cleaved product (Figure S1F). The purity of the human islet and AC preparations was assessed by measuring PDX1 and amylase levels. As previously described, PDX1 protein was detected only in endocrine cells, and the levels were lower in the T2D than the ND islets[25] (Figures 1F and 1G), whereas amylase expression was restricted to ACs (Figures 1F and 1H). CELA3A and CELA3B proteins were clearly expressed in ACs and undetectable in pure β cells (i.e., βH3) (Figures 1F, 1I, and 1J). Intriguingly, both forms of CELA3B protein were detected at significantly high levels in islets from patients with T2D compared with ND preparations (Figures 1F and 1K). Consistently, expression levels of trypsin were also augmented in T2D compared with ND islets (Figure 1F). These results point to the presence of exogenous and active CELA3B within the islets, likely originating in ACs, as endocrine cells do not express the *CELA3B* gene (Figure 1E). The low levels of amylase and other PE proteins in the human islet preparations suggest it is unlikely that the islets, especially those from donors with T2D,

Figure 1. PE expression profile in acinar cell and islets from ND and T2D donors and its effects on β cell viability

(A–E) Transcript levels of (A) *ELANE*, (B) *CELA2A*, (C) *CELA2B*, (D) *CELA3A*, and (E) *CELA3B* genes in the indicated human endocrine and exocrine pancreatic cells and bone marrow (BM). N/d, non-detected. Data are mean ± SEM. One-way ANOVA test was used with Fisher's LSD correction for multiple comparisons.

(F) Representative blots of indicated proteins in human endocrine and exocrine pancreatic cells from ND and T2D donors and human pancreatic elastase (PE). Arrows in the N-CELA3B blot indicate the bands corresponding to the full length (fl) and the cleaved (cl) forms of CELA3B.

(G–K) Quantification of protein levels of indicated proteins from blots in (F). N/d, non detected. Data are mean ± SEM. Two-tailed unpaired t test or one-way ANOVA test with Fisher's LSD correction for multiple comparisons were used.

(L and N) Immunostaining of N-CELA3B (magenta) in the (L) exocrine and (N) endocrine compartment of pancreatic sections of ND (top) or T2D (bottom) donors. Nuclei are stained with DAPI (blue) in (L). Dotted white lines in (N) indicate the border of the islets, labeled with insulin staining (INS, green). Scale bars are indicated in the figure.

(M and O) Quantification of the N-CELA3B signal intensity from (N) exocrine tissue and (O) islets in ND and T2D samples, normalized on the cell area. Data are mean ± SEM. Two-tailed unpaired t test was used.

(P and Q) Representative pictures of confocal imaging to visualize the localization of the cleaved form of CELA3B (N-CELA3B, magenta) within the microenvironment of islets from (P) ND and (Q) T2D pancreas. Insulin (INS, green) was used to label the cytoplasm of β cells, whereas E-cadherin (E-CADH, white) was used to mark cell borders. Nuclei are stained with DAPI (blue). Dotted lines in the insert images were built on top of the E-CADH staining to emphasize the overlap of N-CELA3B with the plasma membranes. Scale bars are indicated in the figure.

(R) Representative images of N-CELA3B distribution in cultured human islets from ND donors following treatment with either PBS (top) or PE at 500 ng/mL (bottom) for 24 h. N-CELA3B is labeled in magenta, whereas insulin (INS) is labeled in green. Scale bars are indicated in the figure.

(S) Experimental design of viability assays in EndoC-βH3 cells following PE treatments.

(T and U) Percentages (%) of (T) EdU^+/$Annexin\ V^+$ cell ratio and (U) caspase-3 activity (% vs. PBS) in EndoC-βH3 cells at the indicated conditions (ng/mL). Data are mean ± SEM. One-way ANOVA test was used with Fisher's LSD correction for multiple comparisons.

(V) Glucose-stimulated insulin secretion assay in perifusion system on EndoC-βH1 pseudoislets treated with either PBS or PE at 500 ng/mL overnight and exposed to 2.8 mM (2.8G) and 16.7 mM (16.7G) glucose concentration. Secreted insulin amounts were normalized on intracellular insulin content, and values at 16.7G were normalized on those at 2.8G to calculate the stimulation index (Y axis). Data are mean ± SEM. Significance vs. PBS was tested using two-way ANOVA test.

See also Figure S1 and Tables S1 and S2.

Please cite this article in press as: Basile et al., Excess pancreatic elastase alters acinar-β cell communication by impairing the mechano-signaling and the PAR2 pathways, Cell Metabolism (2023), https://doi.org/10.1016/j.cmet.2023.05.007

were contaminated by ACs. In addition, the purity of the islet preparations, assessed at the time of isolation, were similar between the T2D and ND samples (Table S1).

To define the precise protein localization of PE within the islet microenvironment, we immunostained pancreas sections from ND and donors with T2D, obtained from the network of pancreatic organ donors (nPOD) repository, for CELA3A and N-CELA3B. Although CELA3A was highly expressed in exocrine tissue and virtually undetectable in ND islets, it was easily detected within islets of T2D pancreatic sections (Figure S1G). By analyzing the abundance and distribution of N-CELA3B protein (the cleaved and active form), we first observed up-regulation in the exocrine tissue of the T2D pancreas compared with the ND samples (Figures 1L and 1M), confirming our gene-expression data (Figure 1E). Additionally, we validated our western blotting results (Figures 1F and 1K) by measuring higher N-CELA3B levels within the islets of the T2D pancreas compared with those from the ND samples (Figures 1N and 1O). Interestingly, the abundance of N-CELA3B within the islets positively correlated with its expression levels in the exocrine compartment of the pancreas, with the ND samples populating the bottom left of the plot (i.e., low N-CELA3B levels in both islets and ACs), and the T2D samples in the top right (i.e., high N-CELA3B levels in both exocrine and endocrine compartments) (Figure S1H). Furthermore, the islet N-CELA3B intensity values were variable among lobules of the same pancreatic sections (Figures S1I and S1K). However, the insulin expression levels were similar in islets across the different regions of the same pancreatic section and globally reduced in T2D vs. ND pancreas (data not shown).

Then we explored the relative localization of N-CELA3B in comparison with insulin and E-cadherin labeling using confocal microscopy. We observed that the N-CELA3B expression pattern was distinct from insulin immunostaining and overlapping with the E-cadherin labeling in both ND and T2D samples (Figures 1P and 1Q), suggesting localization outside the β cells and within the islet microenvironment in both physiological and diabetic states. Taken together, we observed that CELA3B, among the PE forms, was up-regulated in ACs from patients with T2D and its active form was detected in the microenvironment of islets, indicating a potential role in regulating endocrine cell function in diabetes.

Excess of PE within the islet milieu affects β cell homeostasis

To further characterize the effects of PE accumulated in the islet milieu on β cell viability and function, we focused on an *in vitro* model that reproduced the phenotype observed in the human pancreas. To this end, we used isolated ND human islets cultured with either vehicle or exogenous human PE preparations. To estimate the amount of CELA3B present in the islets and sensed by β cells, we used a PE standard curve to quantify the concentration by western blotting. We established that ND islet samples contained CELA3B at ∼150 ng/mL, whereas the T2D islets were exposed to a ∼10-times higher concentration (∼1,000 ng/mL) (Figures S1L and S1M; see STAR Methods). Because the latter concentration was revealed to be unsuitable for our studies in preliminary experiments, we chose 500 ng/mL. Remarkably, the addition of exogenous PE to the islet culture led to accumulation of N-CELA3B in the islet microstructure, recapitulating the conditions observed in the human pancreas of T2D donors (Figures 1N and 1R).

We then sought to determine the effects of exogenous PE on human β cell viability by treating EndoC-βH3 cells with either PBS or PE at low (100 ng/mL) or high (500 ng/mL) concentrations for 24 h (Figure 1S). We observed that the highest dose of PE dramatically reduced viability of β cells, mostly by increasing apoptosis and in part by reducing proliferation (Figures S1N and S1O), resulting in a reduction of the EdU^+/Annexin V^+ cell ratio (Figure 1T). This effect was confirmed by increased caspase-3 activity, which was largely due to PE-induced apoptosis (Figure 1U). Interestingly, the dose of PE found in the ND islets (i.e., 100 ng/mL) significantly decreased proliferation levels without inducing apoptosis and did not alter the β cell numbers (Figures 1T, 1U, S1K, and S1L).

Finally, we tested the effects of PE on β cell function in EndoC-βH1 (βH1) pseudoislets by performing glucose-stimulated insulin secretion (GSIS) assays in a perifusion system. We observed that overnight treatment with PE suppressed glucose responsiveness in β cells (Figure 1V). Taken together, these data showed that exogenous PE, enriched in CELA3B whose levels are increased in T2D islets, affects β cell viability by increasing apoptosis and partially limiting proliferation as well as reducing β cell secretory function. Therefore, blocking the activity of CELA proteins within the islet microenvironment could represent one strategy to promote β cell viability and insulin release in the context of diabetes.

Identification of PE inhibitor compounds

To limit the off-target effects of a broad protease inhibitor such as SerpinB1, which can inhibit elastase as well as proteinase 3 and cathepsin G, we performed high-throughput screenings (HTSs) to test 16,320 DMSO-dissolved small molecules[26–29] using a fluorescence-based porcine PE (pPE) activity assay to identify inhibitors (Figure 2A). After normalizing and scaling the *Z* score values of each compound to DMSO (negative control) and sivelestat (positive control), and adopting the restrictive cut-off of 50% inhibition compared with sivelestat, we identified two FDA-approved drugs as candidate PE inhibitors: (1) telaprevir, an anti-HCV drug, which showed inhibition that was ∼70% higher than sivelestat; and (2) tebipenem, an antibiotic of the β-lactam family, which blocked pPE activity in a similar manner to sivelestat (Figure 2B). We validated these results by testing the efficacy of the candidate compounds in blocking the activity of pPE, human PE, or human neutrophil elastase (NE). We confirmed that telaprevir blocked the activity of both porcine and human forms of PE at low concentrations (IC_{50} pPE: 40.2 nM; IC_{50} PE: 15.8 nM), while tebipenem and sivelestat displayed milder effects (sivelestat IC_{50} pPE: 2.0 μM, IC_{50} PE: 2.3 μM; tebipenem IC_{50} pPE: 107.2 μM, IC_{50} PE: 3.6 μM) (Figures 2C and 2D), reflecting the results of the HTS assay. NE activity was abolished by sivelestat (IC_{50}: 189.1 nM), consistent with previous reports,[30] while telaprevir and tebipenem had a low impact on NE activity (telaprevir IC_{50}: 3.6 μM tebipenem IC_{50}: 33.6 μM) (Figure 2E). None of

Please cite this article in press as: Basile et al., Excess pancreatic elastase alters acinar-β cell communication by impairing the mechano-signaling and the PAR2 pathways, Cell Metabolism (2023), https://doi.org/10.1016/j.cmet.2023.05.007

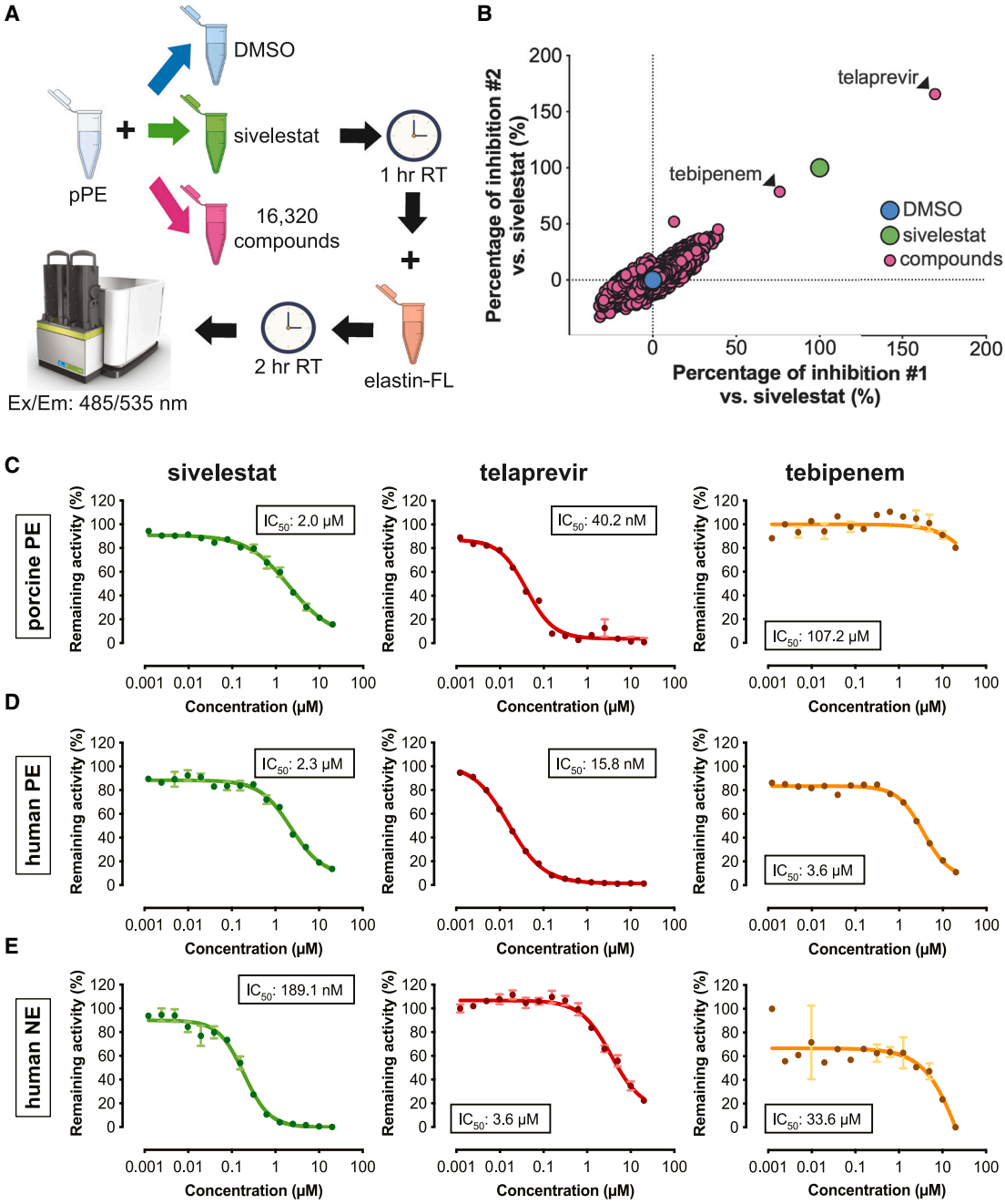

Figure 2. Identification of telaprevir as a specific inhibitor of PE

(A) Experimental scheme of the high-throughput screening (HTS).

(B) Scatterplot of the HTS assay results highlighting the two hits as candidate PE inhibitors.

(C–E) Validation of sivelestat (green curves), telaprevir (red curves), and tebipenem (yellow curves) effect on (C) porcine PE, (D) human PE, and (E) human neutrophil elastase (NE). Data are mean ± SEM (n = 2–4).

See also Figure S1.

the tested compounds inhibited human cathepsin G, at relatively low titers (Figure S1P). The ability of telaprevir to block the activity of PE, with high specificity and at low concentrations compared with other neutrophil proteases, in contrast to sivelestat and tebipenem, prompted us to continue our studies with this compound.

Telaprevir improves human β cell function and viability *in vitro* and *in vivo*

To determine the consequences of inhibiting PE present within the islet microenvironment on human β cell viability, we treated ND human islet cultures for 24 h, either with DMSO or telaprevir (1.5 or 150 μM). The concentrations were selected based on prior

Please cite this article in press as: Basile et al., Excess pancreatic elastase alters acinar-β cell communication by impairing the mechano-signaling and the PAR2 pathways, Cell Metabolism (2023), https://doi.org/10.1016/j.cmet.2023.05.007

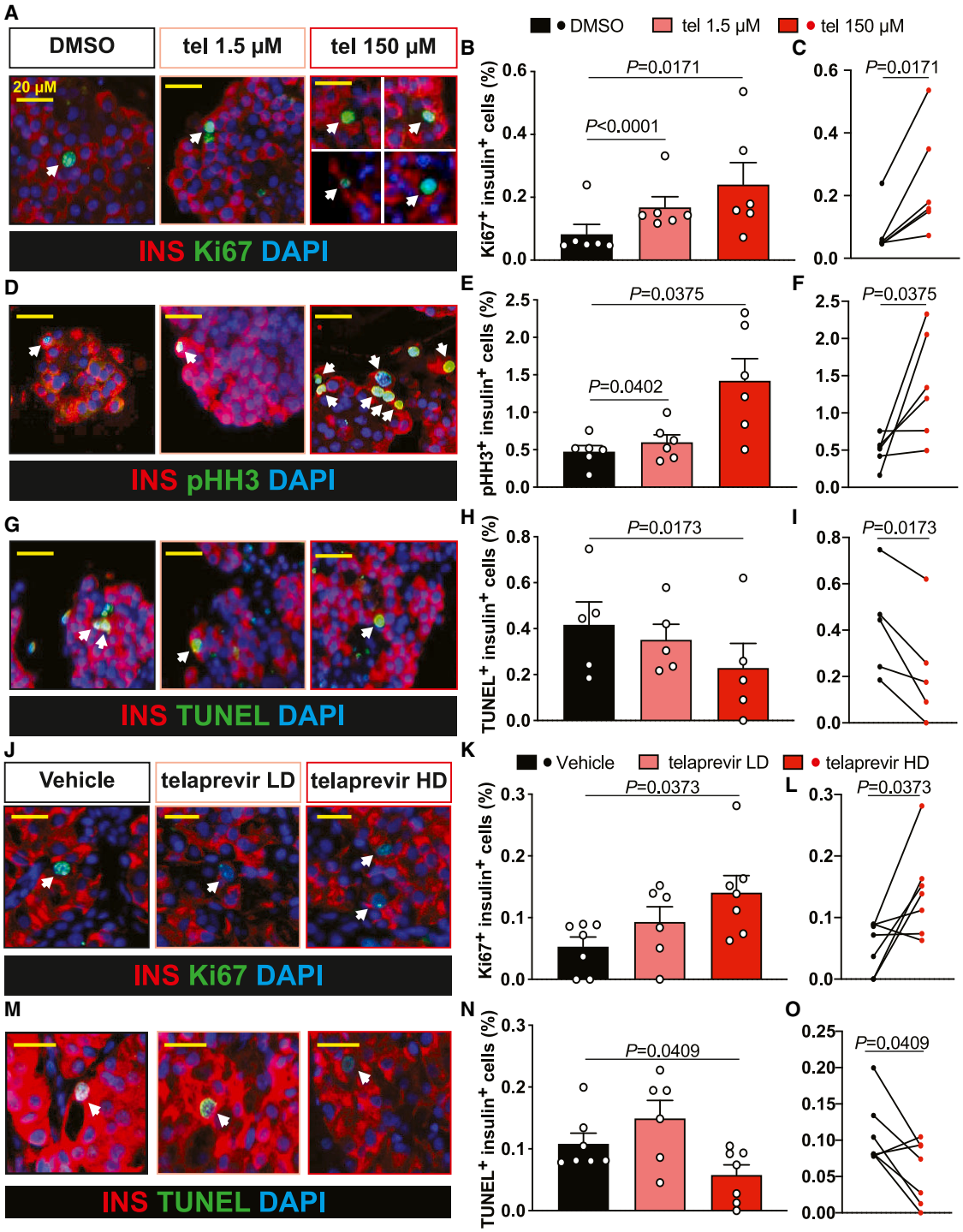

Figure 3. Effects of PE blockade on human β cell viability *in vitro* and *in vivo*

(A, D, and G) Representative picture of (A) Ki67, (D) pHH3, or (G) TUNEL (in green), insulin (in red) and DAPI (in blue) labeling by immunohistochemistry in non-diabetic human islets treated with either DMSO or serial concentrations of telaprevir. Arrows indicate (A and D) proliferating or (G) apoptotic β cells. Scale bars are indicated in the figure.

(B, E, and H) Quantification of (B) Ki67$^+$ insulin$^+$, (E) pHH3$^+$ insulin$^+$, or (H) TUNEL$^+$ insulin$^+$ cell percentage in samples in (A), (D), and (J). Data are mean ± SEM. Paired one-way ANOVA test was used with Fisher's LSD correction for multiple comparisons.

(C, F, and I) Paired analysis of (C) Ki67$^+$ insulin$^+$, (F) pHH3$^+$ insulin$^+$, and (I) TUNEL$^+$ insulin$^+$ cells extrapolated from graphs in (B), (E), and (H). Two-tailed paired t test was used.

(legend continued on next page)

Please cite this article in press as: Basile et al., Excess pancreatic elastase alters acinar-β cell communication by impairing the mechano-signaling and the PAR2 pathways, Cell Metabolism (2023), https://doi.org/10.1016/j.cmet.2023.05.007

studies using elastase inhibitors, such as sivelestat, on promoting human β cell proliferation.[14] Proliferation levels, measured by Ki67 or pHH3 immunolabeling, were significantly increased (~3-fold) in human β cells treated with telaprevir at 100 μg/mL compared with the control (Figures 3A–3F), while apoptosis was also significantly reduced (Figures 3G–3I). Importantly, telaprevir treatment did not stimulate proliferation of other islet cell types, including α-cells (Figures S2A–2C) or δ-cells (data not shown).

To evaluate the beneficial effects of PE inhibition on β cell function, we performed GSIS assays in βH1 cells treated with PE ± telaprevir. Telaprevir was able to counteract the negative effects of exogenous PE and restore glucose responsiveness (Figure S2D). βH1 cells treated with telaprevir in the absence of PE maintained normal function (Figure S2D), indicating that the effect of the compound is dependent on the presence of PE.

To examine the ability of telaprevir to induce human β cell proliferation *in vivo*, we transplanted human islets under the kidney capsule of immunocompromised mice.[31] After allowing islet engraftment for 10 days post-surgery, animals received either vehicle or telaprevir at a low (30 μg/kg/day) or a high (300 μg/kg/day) dose via osmotic pumps for 4 weeks. As for the *in vitro* studies, these dosages were selected based on previous studies.[14] Analysis of human graft samples by immunohistochemistry after 4 weeks of treatment revealed an increase in Ki67$^+$ and a decrease in TUNEL$^+$ β cells in the telaprevir high dose (HD)-treated mice (Figures 3J–3O). However, we did not observe differences between groups in blood glucose (random-fed or fasting) levels, body weight, glucose sensitivity, or human C-peptide levels in fasting states or in response to glucose stimulation (Figures S2E–S2L). The lack of significant changes in these parameters could be due to the brief treatment period and/or the fact that the animals were in a relatively normal physiological state, with intact regulatory mechanisms. Together, these data reveal the mitogenic properties of PE inhibition, mediated by telaprevir, specifically on human β cells in both *in vitro* and *in vivo* systems without inducing hypoglycemia.

PE inhibition increases β cell numbers in models of diabetes

To address the relevance of telaprevir to pathophysiology we began to investigate the effects of PE inhibition on β cell regeneration following diabetes induction using the *Tg(ins:flag-NTR);Tg(tp1:H2BmCherry)* zebrafish model.[32,33] This model is characterized by expressing nitroreductase specifically in insulin-producing cells to promote their ablation upon treatment with metronidazole (Figures S3A and S3B), whereas the duct cells are persistently labeled with the nuclear mCherry fluorescent protein. Either vehicle, sivelestat, or telaprevir were added into the growth medium 4–6 days post-fertilization (dpf). We observed an overall significant increase in Ins$^+$ cells in telaprevir-treated samples compared with controls (Figures S3C and S3D), and a trend toward an increase in larvae treated with sivelestat compared with those treated with DMSO (Figures S3E and S3F). These data confirmed the ability of PE inhibitors to increase β cell numbers *in vivo*.

Then, we focused on mammalian systems to test the potential of telaprevir in promoting β cell viability and restoring glucose homeostasis. To this end, we challenged 4-week-old wild type mice with a 60% fat diet (high fat diet [HFD]), whereas a parallel group was fed on a diet containing 10% fat as a control group (low fat diet [LFD]). After 20 weeks, weight-matched mice fed with the HFD were treated with either vehicle (DMSO) or telaprevir at a low dose (LD) or HD (30 or 300 μg/kg/day, respectively) using osmotic pumps (Figure S4A). Mice fed with the LFD were treated with vehicle to serve as baseline controls. During the treatment period, HFD mice exposed to telaprevir did not exhibit differences in random-fed blood glucose levels or in body weights compared with HFD vehicle-treated animals (Figures S4B and S4C). Interestingly, HFD mice treated with the high dose of telaprevir showed an improvement in glucose tolerance compared with the HFD animals subjected to vehicle at week 4 (Figure S4D). Indeed, the area under the curve during glucose tolerance test (GTT) in HFD telaprevir HD animals was statistically similar to the LFD vehicle group, although not significantly different from vehicle-HFD mice (Figure S4E). Moreover, telaprevir treatment in HFD animals did not affect insulin sensitivity or GSIS compared with the HFD vehicle group at the 4-week time point (Figures S4F and S4G). In addition, telaprevir at HD in HFD conditions lowered the 4 h fasting C-peptide and fasting blood glucose after the 4-week treatment compared with week 0 (Figures S4H and S4I), indicating a limited improvement in glucose homeostasis. Quantification of β cell mass indicated that HFD telaprevir HD mice exhibited a significantly higher β cell mass compared with the HFD vehicle group (Figures S4J and S4K). Interestingly, HFD telaprevir LD and HD mice exhibited slightly lower β cell size compared with the HFD-vehicle group (Figure S4L), suggesting that the increase in β cell mass was likely due to β cell expansion rather than hypertrophy. These data indicate that the blockade of PE activity in insulin-resistant mouse models increased β cell mass and slightly improved glucose tolerance.

PE blockade activates the mechano-signaling and PARs pathways in human islets

To explore the molecular mechanism(s) linking PE activity to β cell viability, we evaluated the phosphoproteomic and transcriptomic changes induced by telaprevir treatment in human islets by phospho-antibody microarrays and single-cell RNA sequencing (scRNA-seq), respectively. In both experiments, we also treated human islets with sivelestat as a positive control

(J and M) Representative picture of (J) proliferating or (M) apoptotic human β cells in humanized models, using (J) Ki67 or (M) TUNEL (in green) and insulin (in red) labeling by immunohistochemistry in transplanted human islets exposed to either vehicle or telaprevir at serial doses. DAPI (in blue) was used to stain nuclei. Arrows indicate (J) proliferating or (M) apoptotic β cells.

(K and N) Quantification of the percentage of (K) Ki67$^+$ insulin$^+$ or (N) TUNEL$^+$ insulin$^+$ cells (Y axis) in samples in (J) and (M). Data are mean ± SEM. Paired one-way ANOVA test was used with Fisher's LSD correction for multiple comparisons.

(L and O) Paired analysis of (L) Ki67$^+$ insulin$^+$ or (O) TUNEL$^+$ insulin$^+$ cells extrapolated from graphs in (K) and (N). Two-tailed paired t test was used.

See also Figure S2 and Table S1.

Please cite this article in press as: Basile et al., Excess pancreatic elastase alters acinar-β cell communication by impairing the mechano-signaling and the PAR2 pathways, Cell Metabolism (2023), https://doi.org/10.1016/j.cmet.2023.05.007

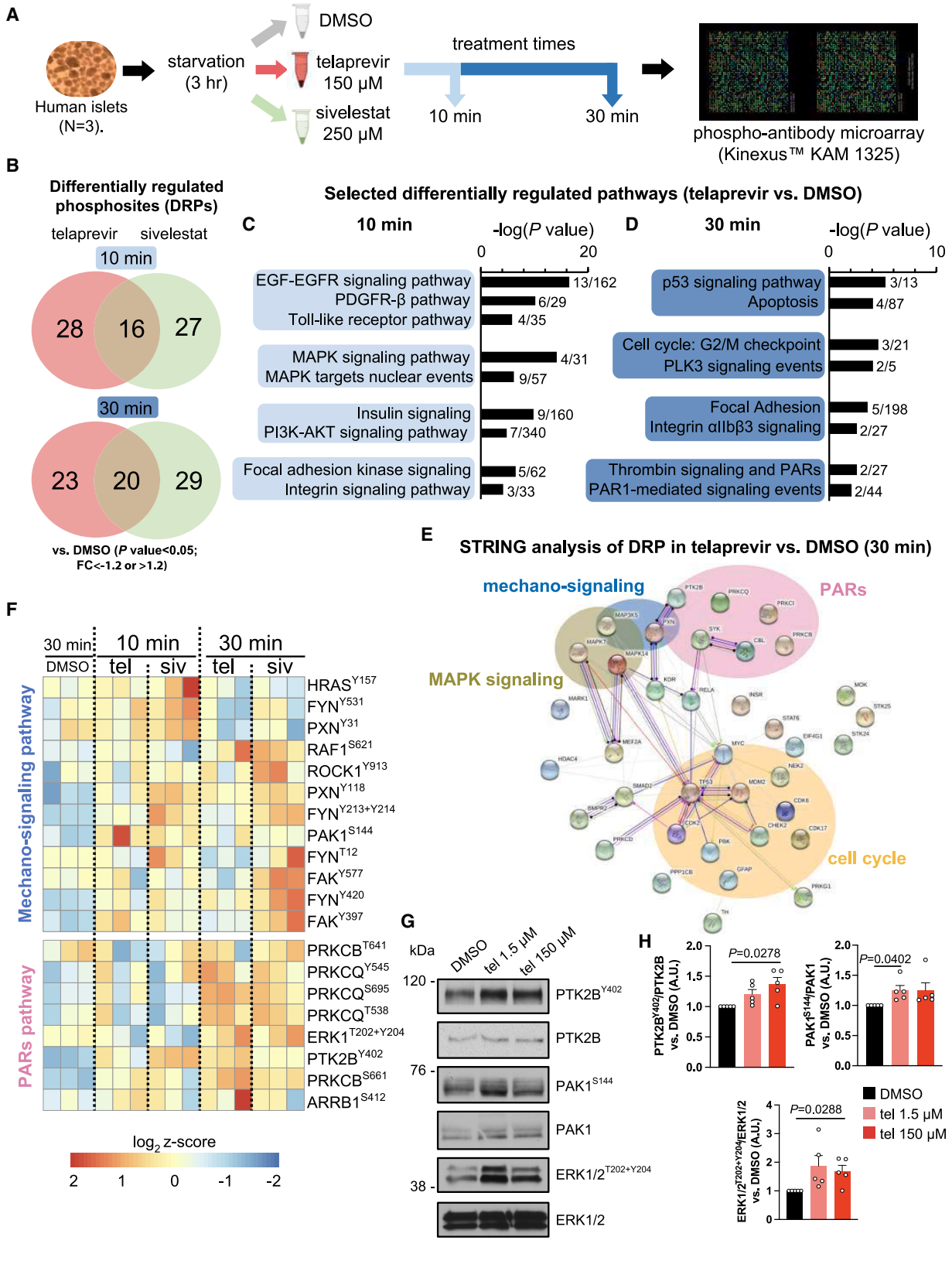

(legend on next page)

Please cite this article in press as: Basile et al., Excess pancreatic elastase alters acinar-β cell communication by impairing the mechano-signaling and the PAR2 pathways, Cell Metabolism (2023), https://doi.org/10.1016/j.cmet.2023.05.007

for the inhibition of PE (Figures 2C and 2D). To identify the signaling pathways, we incubated human islets with DMSO, telaprevir, or sivelestat for 10 or 30 min, after which protein lysates were submitted to KAM 1325 microarrays (Kinexus, Canada) (Figure 4A) to interrogate the expression and phosphorylation states of key cell signaling proteins simultaneously. Using p value < 0.05 and fold change (FC) $\gtrless|1.2|$ as cutoffs, we observed 44 and 43 (10-min treatment), and 43 and 49 (30-min treatment) differentially regulated phosphosites (DRPs) in human islets treated with telaprevir or sivelestat, respectively (Figure 4B). The two elastase inhibitors shared ~50% of the regulated phosphosites at both time points, highlighting the presence of common elastase-specific effects. Pathway analysis revealed that MAPK and PI3K-AKT signaling were regulated by both telaprevir and sivelestat after 10- and 30-min treatment, respectively, consistent with our previous studies on SerpinB1,[14] in addition to growth factor signaling cascades driven by EGFR, PDGFR, and the insulin receptor (Figures 4C, S5A, and S5B). Interestingly, the integrin and focal adhesion pathways, two major networks that integrate mechano-signals originating from the extracellular environment, were differentially regulated by both telaprevir and sivelestat at 10 as well as 30 min, underlining a role for PE in regulating the mechano-signaling machinery responsible for ECM-cell interactions (Figures 4C, 4D, S5A, and S5B). Finally, both compounds regulated cell cycle and proliferation-related pathways, as well as apoptosis and p53 signaling events, confirming the link between elastase blockade and growth in human islet cells (Figures 4D, S5A, and S5B). Notably, sivelestat specifically regulated Hippo and VEGF signaling and the leptin pathways (Figures S5A and S5B).

The PARs signaling cascade was significantly modulated by stimulation with telaprevir, but not sivelestat, at 30 min, suggesting a distinct consequence of selective PE inhibition by the former (Figures 4D, S5A, and S5B). Further interrogation of top DRPs by STRING (Search Tool for the Retrieval of Interacting Genes/Proteins) analyses suggested interconnections between MAPK, mechano-signaling, and PARs pathways with the cell cycle network in telaprevir-treated samples (Figure 4E). Further analysis of the integrin/focal adhesion pathway revealed that phosphorylation levels of paxillin (PXN) at Tyr118 and Tyr31 residues, and p21 (RACs1) activated kinase 1 (PAK1) at Ser144, were higher following PE inactivation, suggesting activation of the focal adhesion machinery (Figure 4F). In parallel, telaprevir increased the phosphorylation levels of protein tyrosine kinase 2B (PTK2B) at the Tyr402 site, and extracellular-signal-regulated kinase 1/2 (ERK 1/2) at the Thr202 and Tyr204 sites, leading to the activation of PARs signaling (Figure 4F). We validated the results by western blotting, using human islets treated with telaprevir (1.5 or 150 μM for 30 min). Consistent with the previous data, phosphorylation levels of PAK1 in the mechano-signaling pathway and PTK2B and ERK1/2, downstream effectors of the PARs signaling cascade were all up-regulated by telaprevir (Figures 4G and 4H). Taken together, these experiments suggest that PE: (1) interrupts the ECM-cell interactions to inactivate the mechano-signaling machinery and (2) inhibits PARs signaling. Furthermore, a significant correlation of these pathways with cell cycle networks linked PE inhibition to growth processes.

Single-cell RNA-seq analysis reveals the impact of PE on the mechano-signaling and PARs pathways in human β cells

We then examined the transcriptomic profile of human islet cells, following incubation with telaprevir or sivelestat for 24 h, to assess the β cell-specific effects of sustained PE inhibition. scRNA-seq (Figure 5A) recovered 1,199, 3,194 and 1,656 high-quality cells from human islets treated with DMSO, telaprevir, or sivelestat, respectively (Table S3). Following deconvolution and cell cluster definition using the expression levels of gene markers of pancreatic cell types, we obtained 157, 456, and 338 β cells in the samples treated with DMSO, telaprevir, or sivelestat, respectively (Figures 5B and S6A–S6H; Table S3). Differential gene-expression analyses revealed that 410 and 261 genes were significantly up-regulated in β cells in samples treated with telaprevir and sivelestat, respectively (Figure 5C). These included ribosomal protein S27 (*RPS27*), pancreatic progenitor cell differentiation and proliferation factor (*PPDPF*), solute carrier family 30 member 8 (*SLC30A8*; known as Zn^{2+} transporter ZnT8), and receptor for activated C kinase 1 (*RACsK1*) in telaprevir-treated samples, and ribosomal protein S29 (*RSP29*) and actin gamma 1 (*ACsTG1*) in samples treated with sivelestat (Figures 5D and 5E). Moreover, 161 and 184 genes were differentially down-regulated in β cells of samples treated with telaprevir or sivelestat, respectively (Figure 5C). Among them, proprotein convertase subtilisin/kexin type 1 inhibitor (*PCSK1N*) and β-2 microglobulin (*B2M*) were significantly down-regulated in both telaprevir- and sivelestat-treated human β cells (Figures 5D and 5E). Canonical pathway analysis performed within the β cell dataset indicated an up-regulation of pathways important for proliferation such as DNA replication and G1/S transition, confirming the mitogenic properties of PE inhibition (Figure 5F). Unexpectedly, telaprevir positively regulated β cell identity genes (Figure 5F). In line with these data, exocrine-cell-specific pathways, including Notch signaling and Hippo pathways, were down-regulated by telaprevir in acinar and ductal cells compared

Figure 4. Results of phospho-antibody microarrays in human islets following telaprevir-mediated PE inhibition

(A) Experimental design of phospho-antibody microarray experiments.

(B) Differentially regulated phosphosites (DRPs) in human islets treated with telaprevir (red circles) and sivelestat (green circles) for 10 min (upper circles) or 30 min (lower circles).

(C and D) Selected differentially regulated pathways in human islets treated with telaprevir at (C) 10 min or (D) 30 min.

(E) STRING analysis showing network of proteins differentially phosphorylated by telaprevir at 30 min.

(F) Selected heatmaps of differentially regulated phosphosites belonging to the mechano-signaling or PARs pathways in human islets at the indicated conditions.

(G) Representative blots of indicated phosphorylated and total proteins in human islets at the indicated conditions.

(H) Quantification of the indicated phosphorylated protein levels from blots in (G). Data are mean ± SEM. One-way ANOVA test was used with Fisher's LSD correction for multiple comparisons.

See also Figure S5 and Table S1.

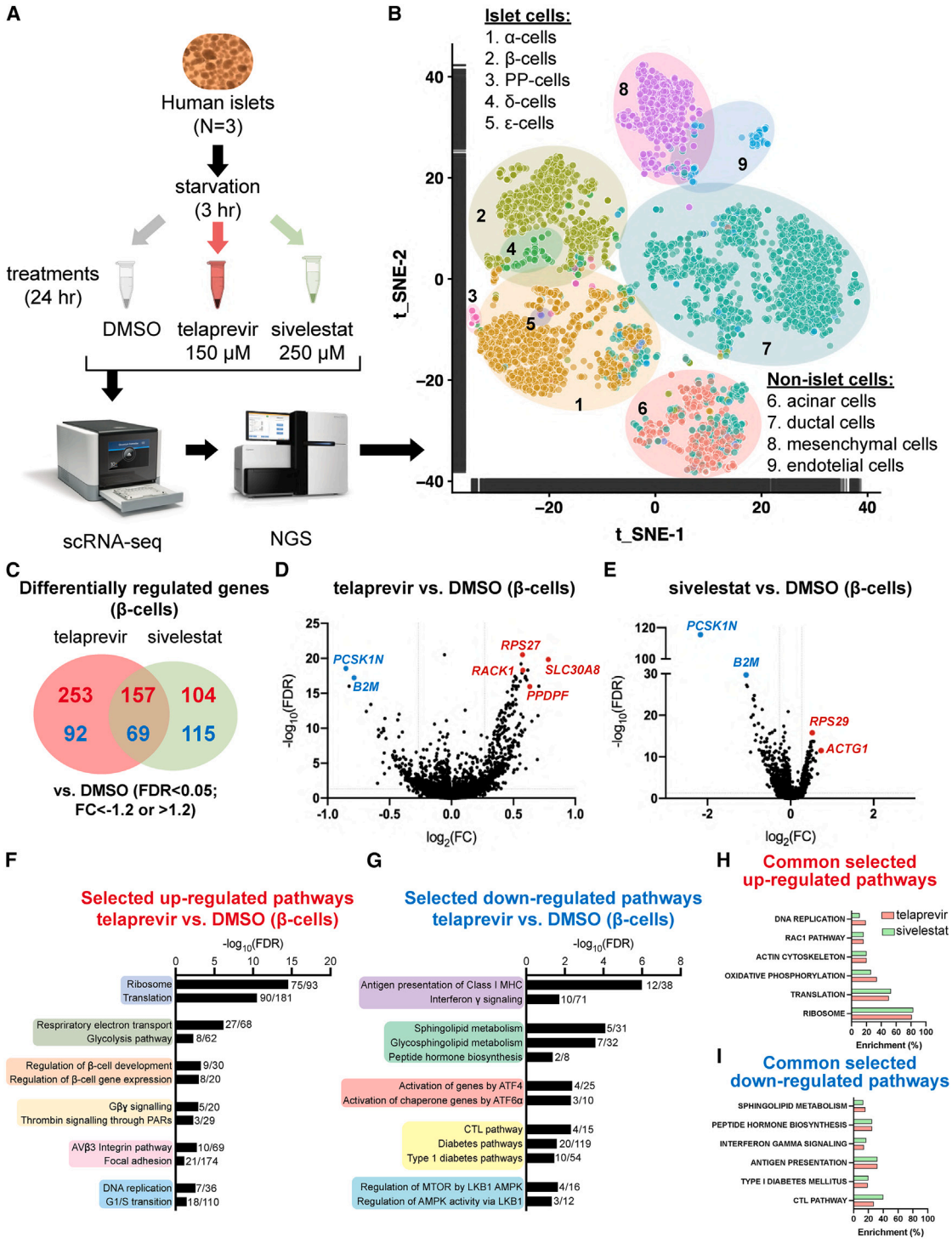

Figure 5. Transcriptomic changes in human β cells regulated by telaprevir-dependent PE blockade

(A) Experimental design of single-cell RNA sequencing (scRNA-seq) experiments.

(B) Global t_SNE plot representing the dispersion of the high-quality cells, including all three experimental groups.

(C) Differentially up-regulated (in red) and down-regulated (in blue) genes in human islets treated with telaprevir (red circle) or sivelestat (green circle).

(D and E) Volcano plots of differentially regulated genes in β cells treated with (D) telaprevir and (E) sivelestat compared with DMSO.

(F and G) Selected differentially (F) up-regulated and (G) down-regulated pathways in human β cells treated with telaprevir vs. DMSO.

(H and I) Selected differentially (H) up-regulated and (I) down-regulated pathways shared by β cells treated with telaprevir and sivelestat. Data are percentage of enrichment of differentially regulated genes.

See also Figure S6 and Tables S1, S3, and S4.

Please cite this article in press as: Basile et al., Excess pancreatic elastase alters acinar-β cell communication by impairing the mechano-signaling and the PAR2 pathways, Cell Metabolism (2023), https://doi.org/10.1016/j.cmet.2023.05.007

with DMSO-treated samples (Figure S6I), suggesting a link between PE activity and β cell maturation/differentiation.

AVβ3 integrin, focal adhesion and PARs pathways were differentially up-regulated by telaprevir, consistent with the phospho-antibody microarray results, emphasizing the importance of these signaling axes in the regulation of PE-mediated β cell growth (Figure 5F). Notably, actin remodeling and DNA replication pathways were also up-regulated in sivelestat-treated β cells, whereas regulation of genes in PARs signaling appeared specific to telaprevir treatment (Figures 5F and 5H). The focal adhesion and the PARs pathways were down-regulated in other cell types, including acinar, ductal, and α-cells (Figure S6I), indicating that the up-regulation of such pathways was specific to the β cells. Genes belonging to antigen presentation by class I major histocompatibility complex (MHC) and T1D pathways were down-regulated in human β cells treated with telaprevir (Figure 5G), pointing to the relevance of PE inhibition in the context of T1D. The down-regulation of the T1D-related pathways was shared by sivelestat-treated samples (Figure 5I). Finally, the inhibition of PE function resulted in cell stress relief, as the activating transcription factor (ATF) 6α and ATF4 pathways were significantly down-regulated by telaprevir (Figure 5G).

By integrating the phospho-antibody microarray data with the scRNA-seq dataset of the β cells, we focused on transcription factors that were differentially phosphorylated in human islets treated with telaprevir compared with DMSO and linked them to the changes in gene expression observed in telaprevir-treated β cells. This allowed us to create a network map integrating the global regulation of telaprevir in β cells at both phospho-proteomic and transcriptomic levels (Figure S6J). For example, we observed that telaprevir regulated genes involved in cell cycle signaling, such as the G1/S transition pathway, likely by modulating the activity of JUN, whereas genes defining β cell identity, grouped in the maturity-onset diabetes of the young (MODY) pathway, were regulated likely via TP53 (Figure S6J). Using this approach, we observed that the expression of genes involved in the actin remodeling pathways, which were differentially up-regulated by telaprevir in human β cells, was controlled by transcription factors such as MYC, RELA, or CTNBB1, and differentially phosphorylated upon telaprevir treatment (Table S4). Taken together, these data provide insight into pathways (e.g., mechano-signaling and PARs pathways) that are regulated following PE inhibition and precede the up-regulation of the cell cycle machinery in β cells.

Human islets from patients with T2D exhibit impaired PAR2 and mechano-signaling pathways

To evaluate the translational relevance of our findings, we examined the protein expression of FAK, PTK2B, and the PARs known to be expressed in pancreatic islets[22,23] (i.e., PAR2 and PAR3), in βH3 cells and human islets from ND and T2D donors (Figure 1F). Expression of FAK (Figures 6A and 6B) and proteins in the PARs pathway, including PTK2B and PAR2, were lower in T2D samples compared with ND (Figures 6A, 6C, and 6D). However, PAR3 expression was not significantly different between groups (Figures 6A and 6E), highlighting PAR2 as a target that may be regulated by PE. These data suggest that the mechano-signaling and PAR2 pathways, which are up-regulated by PE inhibitors, are impaired in T2D islets in the presence of high levels of CELA3B (Figures 1F and 1K).

PE affects the PAR2 signaling pathway in β cells

Elastase causes non-canonical proteolytic cleavage of PAR2.[21,34] To investigate the effects of PE and PE inhibition on PAR2 signaling, we interrogated the phosphorylation of ERK1/2, an important effector downstream of the PAR2 signaling cascade,[35] in βH1 cells pre-treated with FSLLRY-NH_2, a PAR2-inactivating peptide, and subsequently stimulated with PE ± telaprevir for 30 min (Figure 6F). Although cells treated with PE did not exhibit changes in phospho-ERK1/2 levels compared with control cells, PE inhibition by telaprevir significantly increased phospho-ERK1/2 levels (Figures 6G and 6H). Remarkably, such an effect was not observed in cells pre-treated with FSLLRY-NH_2 (Figures 6G and 6H), indicating that the ERK activation caused by telaprevir-dependent inhibition of PE is mediated by the PAR2 pathway.

To evaluate whether the regulation of PE on PAR2 signaling impacted β cell viability, we evaluated proliferation and apoptosis levels in primary human β cell cultures, obtained by dispersing islets, pre-incubated with or without FSLLRY-NH_2 and subsequently treated with PE ± telaprevir for 24 h. Human β cells were labeled with diacetylated Zinpyr1 (DA-ZP1), a previously characterized zinc-binding molecule conjugated with GFP[36,37] (Figure 6I). We confirmed that PE caused a non-significant decrease in β cell viability compared with control cells, whereas the addition of telaprevir significantly improved β cell survival (Figure 6J). Although the PAR2 inhibitor did not affect β cell homeostasis compared with vehicle-treated cells, the capacity of telaprevir to counteract the detrimental effects of PE was impaired in FSLLRY-NH_2-treated cells (Figure 6J), pointing to the PAR2 signaling pathway as one of the molecular links between PE activity and β cell homeostasis.

PE inhibits the mechano-signaling axis in β cells

To understand whether the integrin/focal adhesion axis is an essential component of telaprevir-mediated PE inhibition, we knocked down focal adhesion kinase (FAK), the protein immediately downstream of the integrin receptor along the mechano-signaling pathway, in βH1 cells by transient interference experiments to obtain siFAK cells. Cells transfected with non-specific oligo (scramble cells) or siFAK cells (Figure S7A) were then treated with either PBS or PE, without or with telaprevir, at increasing doses for 30 min, and the phosphorylation of PAK1 protein, which directs the integrin signaling to cytoskeleton remodeling,[38] was analyzed by western blotting (Figure 7A). We observed a significant reduction of phospho-PAK1 levels in PE- vs. PBS-treated scramble cells (Figures 7B and 7C). Importantly, telaprevir reversed the PE-dependent effects by significantly increasing phosphorylation of PAK1 in scramble cells stimulated with PE + telaprevir at HD, in comparison with scramble cells incubated with PE alone (Figures 7B and 7C), suggesting that the stimulatory effect of telaprevir on the mechano-signaling pathway is mediated by PE inhibition. On the other hand, FAK down-regulation caused a significant reduction of PAK1 phosphorylation levels compared with those of scramble cells (Figures 7B and 7C).

Please cite this article in press as: Basile et al., Excess pancreatic elastase alters acinar-β cell communication by impairing the mechano-signaling and the PAR2 pathways, Cell Metabolism (2023), https://doi.org/10.1016/j.cmet.2023.05.007

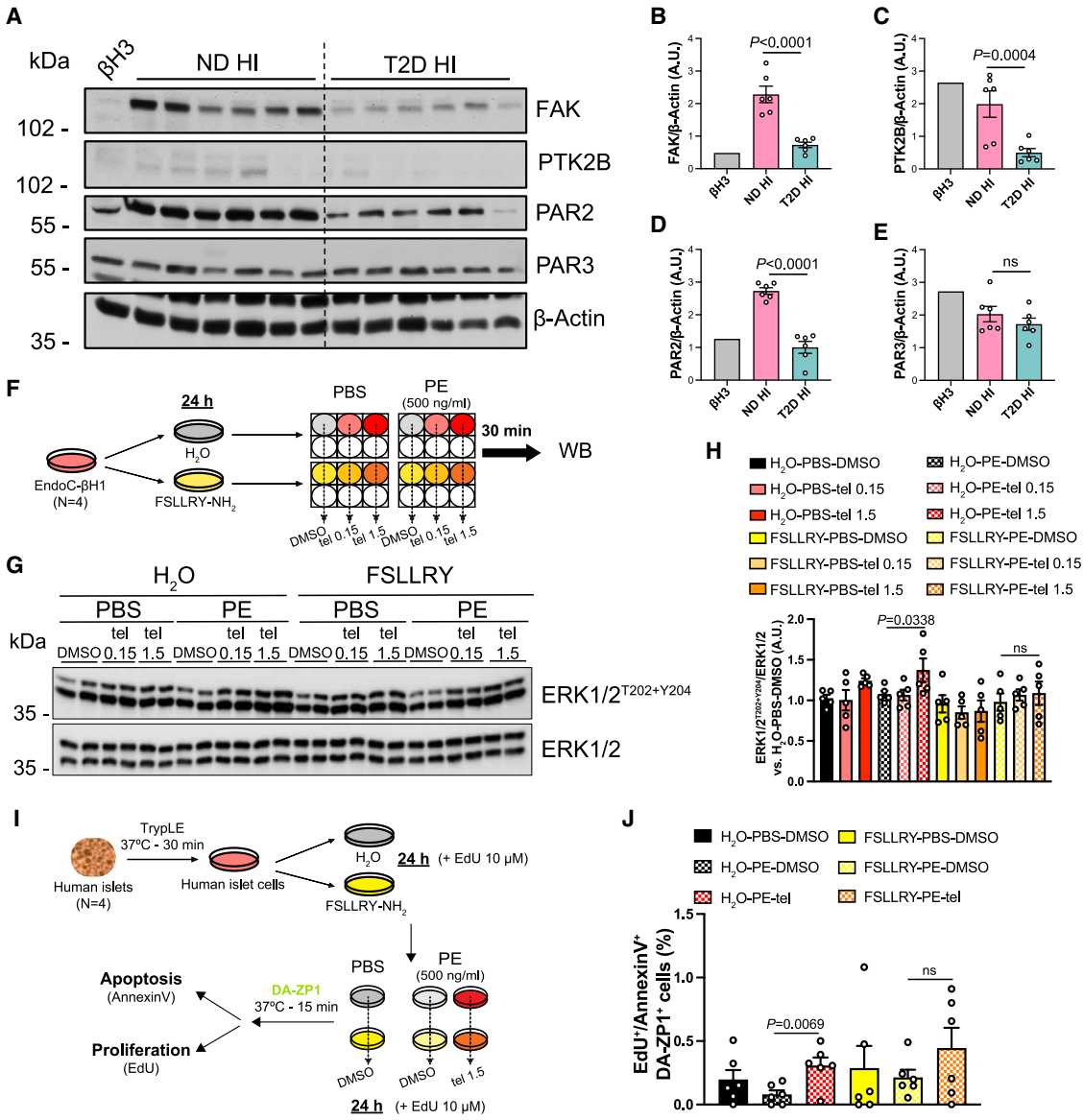

Figure 6. Levels of proteins along the candidate pathways in islets of donors with T2D and effects of PE on the PAR2 signaling in human islets and human β cells

(A) Representative blot of indicated proteins in pancreatic islet cells from ND and T2D donors. Western blotting experiment is from Figure 1F.

(B–E) Quantification of indicated protein levels from blots in (A). Data are mean ± SEM. One-way ANOVA test was used with Fisher's LSD correction for multiple comparisons.

(F) Scheme of the experimental design of stimulations in EndoC-βH1 cells to investigate the PAR2 pathway.

(G) Representative blots of phosphorylated and total ERK1/2 protein levels in EndoC-βH1 at the indicated conditions.

(H) Quantification of phospho-ERK1/2 levels from blots in (G). Data are mean ± SEM. One-way ANOVA test was used with Fisher's LSD correction for multiple comparisons. Ns, non-significant

(I) Experimental design of viability assays in human islet cells following PAR2 receptor blockade.

(J) Quantification of the EdU$^+$/Annexin V$^+$ cell percentage within the DA-ZP1$^+$ cell population (β-cells) at the indicated conditions. Ns, non-significant. Data are mean ± SEM. One-way ANOVA test was used with Fisher's LSD correction for multiple comparisons.

See also Table S1.

Finally, the combination of telaprevir with PE in siFAK cells significantly decreased phosphorylated PAK1 compared with PE-treated siFAK samples, showing an opposite effect to scramble cells (Figures 7B and 7C). These results suggest that PE is a negative regulator of the mechano-signaling axis in β cells and that these effects are restored after PE is inhibited by telaprevir.

To define the effects of PE on the mechano-signaling pathway in β cells, we conducted gain-of-function experiments by overexpressing FAK in βH1 cells using a FLAG-tagged

Please cite this article in press as: Basile et al., Excess pancreatic elastase alters acinar-β cell communication by impairing the mechano-signaling and the PAR2 pathways, Cell Metabolism (2023), https://doi.org/10.1016/j.cmet.2023.05.007

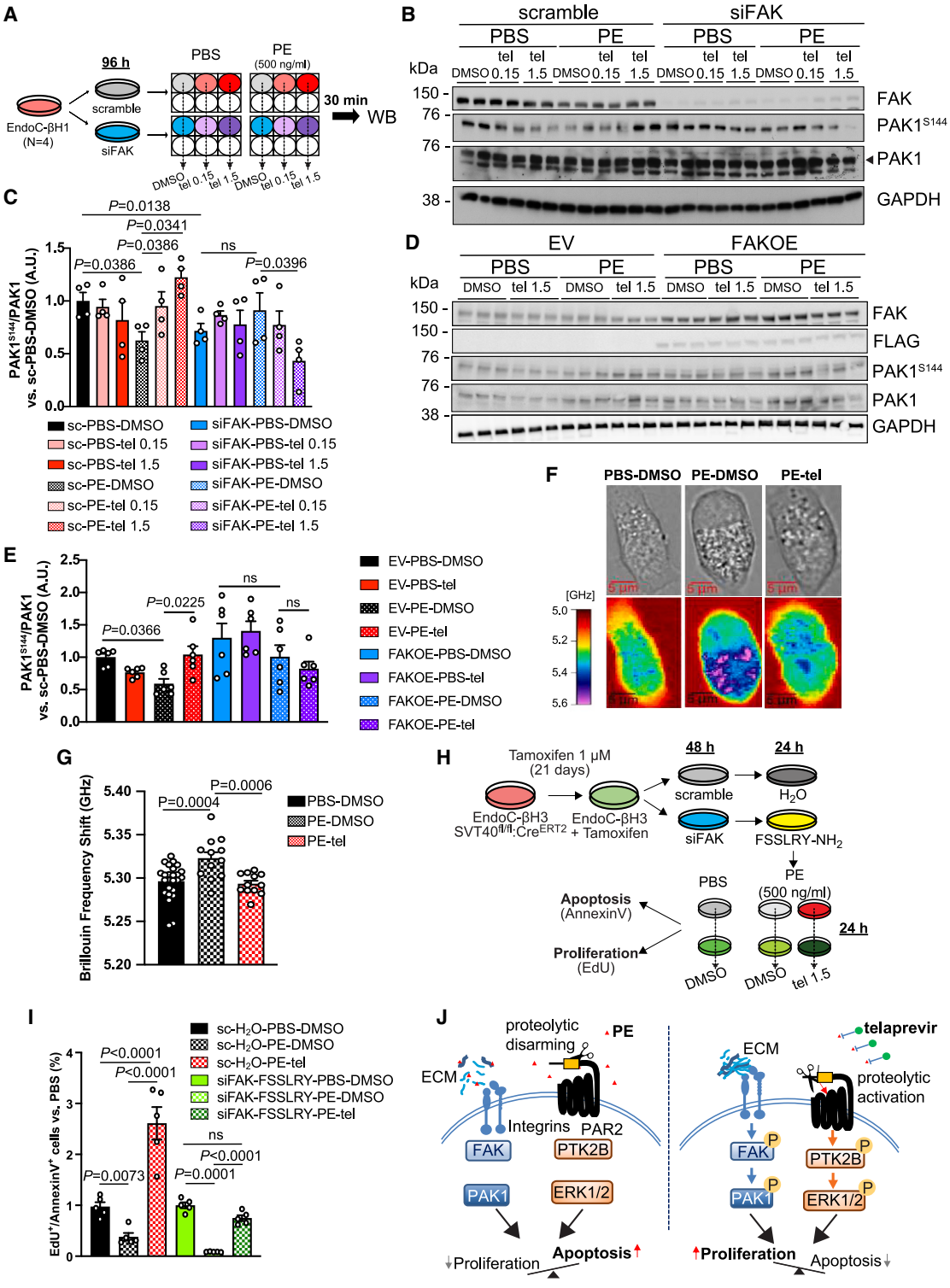

Figure 7. Effects of PE on the mechano-signaling pathway in human β cells

(A) Experimental scheme of stimulations in EndoC-βH1 cells to investigate the mechano-signaling pathway.

(B and D) Representative blots of phosphorylated and total PAK1 protein levels in EndoC-βH1 in which FAK expression was (B) down-regulated or (D) up-regulated and stimulated at the indicated conditions.

(C and E) Quantification of phospho-PAK1 levels from blots in (B) and (D). Data are mean ± SEM. One-way ANOVA test was used with Fisher's LSD correction for multiple comparisons. Ns, non-significant.

(legend continued on next page)

Please cite this article in press as: Basile et al., Excess pancreatic elastase alters acinar-β cell communication by impairing the mechano-signaling and the PAR2 pathways, Cell Metabolism (2023), https://doi.org/10.1016/j.cmet.2023.05.007

construct. Cells transfected with either an empty vector (EV) or FAK (FAKOE) (Figures S7B and S7C) were then stimulated with either PBS or PE in combination with either DMSO or telaprevir. We confirmed that phospho-PAK1 levels were reduced by PE treatment and restored by the addition of telaprevir in EV cells (Figures 7D and 7E). Overexpression of FAK per se caused a non-significant increase in phospho-PAK1 levels, and this increment was not altered by PE alone or PE in combination with telaprevir (Figures 7D and 7E). These results indicate that increasing the expression of FAK in β cells counteracts the detrimental effects of PE, confirming the mechano-signaling pathway among the molecular mechanism(s) targeted by PE activity.

PE alters the mechanical state of β cells

To evaluate whether the PE-mediated impairment of the mechano-signaling cascade impacts the cytoskeleton dynamics of the β cells, we interrogated the mechanical state of βH1 cells exposed to PE, with or without telaprevir, by using Brillouin microscopy, an emerging technology developed to measure the stiffness of cells, as a readout of cytoskeleton remodeling.[39] We initially observed that cells treated with PE were more circular than control cells, whereas the shape of cells incubated with PE in the presence of telaprevir resembled the PBS-treated cells (Figure 7F). By measuring the Brillouin frequency shift to infer the cytoskeleton assembly state, we observed that PE-treated cells had a significant higher Brillouin frequency shift, indicating a higher stiffness compared with control cells (Figures 7F and 7G). Remarkably, telaprevir was able to completely reverse these effects (Figures 7F and 7G). These results suggest that chronic exposure to PE, which reduces β cell viability, increases the intracellular stiffness of β cells, likely because of interrupted interactions between the ECM and integrins.

PE reduces β cell viability by inhibiting the PAR2 and mechano-signaling pathways

To explore the relationship between the PE-mediated effects on the candidate pathways (i.e., the mechano-signaling and PAR2 pathway) and β cell viability, we measured proliferation and cell death parameters following PE inhibition in cells in which both pathways were simultaneously impaired. To this end, we used tamoxifen-treated βH3 cells to generate scramble or siFAK cells (Figures S7D and S7E), which were further incubated with either vehicle or FSSLRY-NH_2, respectively (Figure 7H). We observed that PE treatment significantly decreased the proliferation/apoptosis ratio in scramble cells (Figure 7I), which confirmed our earlier results (Figure 1T). Interestingly, the inhibition of PE mediated by telaprevir boosted β cell viability levels even higher than control cells (Figure 7I). This was the result of a slight effect on restoring PE-mediated decrease of proliferation levels together with a major effect in counteracting PE-dependent apoptosis (Figures S7F and S7G). Blockade of both pathways reduced β cell proliferation levels, without a significant effect on overall cell viability, compared with scramble cells (Figures 7I, S7F, and S7G). Interestingly, incubation of these cells with PE further reduced proliferation and increased apoptosis levels, determining a profound loss of β cells (Figures 7I, S7F,and S7G). Finally, inhibition of PE using telaprevir restored regeneration levels and survival of siFAK-FSLLRY-treated cells (Figures 7I, S7F, and S7G). However, the proportion of viable cells in the siFAK-FSSLRY group was non-significantly different to those treated with vehicle, contrary to the dynamic pattern occurring in control cells (Figures 7I, S7F, and S7G). Thus, our studies in βH and human islet cells suggest that the mechano-signaling axis and the PAR2 signaling are potential mediators of the effects of PE activity on β cells, leading to poor viability (Figure 7J).

DISCUSSION

Pancreatic islets are surrounded by ACs that synthesize and secrete enzymes to promote digestion of nutrients in the intestine.[40] In addition, ACs are able to secrete proteins directly into the circulation as well as into the pancreatic stroma to impact islet cell homeostasis in physiological and pathophysiological states.[41–43] Of relevance to this report, PE represents one such candidate, as fecal PE levels are altered in patients affected by various forms of diabetes.[17,44]

Here, we discovered that the expression of one of the major forms of PE, namely *CELA3B*, retained in exocrine cells and virtually null in either pure β cells or human islets, was up-regulated in ACs from patients with T2D compared with ND samples. Surprisingly, we then observed that the protein levels of both the proenzyme and active forms of CELA3B were higher in T2D human islets compared with ND. The observation of accumulation of cleaved CELA3B in T2D samples could be explained by the presence of trypsin within the islet milieu, an AC-specific enzyme previously identified as a regulator of acinar-to-islet communication.[42] By overexposing the amylase blot, we noted that at least one ND islet preparation showed high levels of CELA3B, likely due to contaminant ACs in the sample. However, we excluded the notion that the detection of both full-length and cleaved forms of CELA3B protein in the T2D islet preparations was due to contamination of exocrine cells as well as from potential dedifferentiation usually observed in β cells from T2D,[45] based on the following observations: (1) AC marker genes were absent in endocrine cells; (2) the expression of exocrine-specific proteins

(F) Representative bright-field (upper) and Brillouin imaging (lower) pictures of EndoC-βH1 cells treated with either vehicle solutions (PBS-DMSO, left) or PE (middle), or PE with telaprevir (right), for 24 h. Brillouin shift heatmap is expressed in GHz and ranges from 5 (red, low stiffness) to 5.6 (purple, high stiffness).
(G) Quantification of Brillouin frequency shift from pictures in (A). Data are mean ± SEM. One-way ANOVA test was used with Fisher's LSD correction for multiple comparisons.
(H) Experimental design of viability assays in EndoC-βH3 cells upon treatments with PE in combination or not with telaprevir.
(I) Quantification of the EdU^+/Annexin V^+ cell ratio in EndoC-βH3 cells at the indicated conditions. Data are mean ± SEM. One-way ANOVA test was used with Fisher's LSD correction for multiple comparisons. Ns, non-significant.
(J) Working model of the mechanism of action of telaprevir on β cell viability by modulating the mechano-signaling and PAR2 pathways.
See also Figure S7.

Please cite this article in press as: Basile et al., Excess pancreatic elastase alters acinar-β cell communication by impairing the mechano-signaling and the PAR2 pathways, Cell Metabolism (2023), https://doi.org/10.1016/j.cmet.2023.05.007

(i.e., amylase and CELA3A), although detectable at low levels in human islet samples, does not correlate with the amount of CELA3B and N-CELA3B; and (3) the purity of the human islet preparations obtained from T2D donors was similar to those of ND human islets (>80%). The presence of the high levels of the active form of CELA3B protein, detected using an antibody specific for its cleaved form, within the microenvironment of islets in pancreatic samples, argues that PE is secreted from ACs into the exocrine-endocrine interface with the potential to act in a paracrine fashion on β cells. The ability of PE enriched in CELA3B to decrease the viability of βH3 cells by lowering the proliferation/apoptosis ratio, mainly by inducing caspase-3 activation-mediated cell death, suggested that the elevated PE likely contributes to the deficit in β cell numbers in patients with diabetes.[2] Interestingly, the null effect on apoptosis of PE at lower concentrations suggests that physiological concentrations of PE in the islet microstructure of ND individuals would prevent β cells from replicating without impacting their viability. In addition, the all-or-nothing mechanism of action of PE, especially in regulating apoptosis, suggests that β cells tolerate the presence of PE in their surrounding up to a threshold (e.g., 200–500 ng/mL). These data, together with the observation that insulin release was suppressed by PE at the concentration found in T2D islets, supports a broader role of PE in regulating β cell homeostasis at multiple levels.

We further explored pharmacological inhibition of PE on β cell viability by using telaprevir, an FDA-approved drug identified as a major hit from a HTS assay. An advantage of telaprevir is its ability to specifically inhibit human PE, while displaying virtually no effect on other protease targets of SerpinB1 activity (e.g., cathepsin G). Treating cultured and transplanted human islets with telaprevir led to a β cell-specific increase in proliferation and survival levels. Furthermore, telaprevir blocked the detrimental effects of PE and restored GSIS in β cells. Although telaprevir at high concentrations (>10 μM) is able to partially inhibit human NE activity, we exclude that its effects on β cell growth are secondary to NE blockade as its gene is not expressed in human islet preparations. In addition, neutrophil cells are virtually absent in human islets, even in disease states as T2D, as they were undetected in our and published scRNA-seq datasets.[46–48] HFD-fed mice treated with telaprevir exhibited a little improvement in glucose tolerance, likely secondary to the expansion of β cell mass. Consistent with a study that has reported that rapid β cell growth is linked to a loss of maturity and function,[49] we observed that the new β cells generated by self-replication following telaprevir treatment in HFD mice also did not respond to glucose stimulation *in vivo*. However, the lower C-peptide levels observed after 4 weeks of telaprevir therapy is a likely consequence of adaptation of β cells to low fasting blood glucose levels rather than a negative effect of telaprevir on β cell function or maturity. The lack of alterations in insulin sensitivity in telaprevir-treated HFD mice excluded side-effects of the compound on other metabolic tissues, such as liver, adipose tissue, or muscle. These data point to the safety and efficacy of PE blockers in improving glucose homeostasis in *in vivo* models.

Phospho-antibody arrays and scRNA-seq experiments on telaprevir-treated human islets revealed (1) the mechano-signaling and (2) the PARs pathway as molecular links between PE activity and poor β cell viability. Interestingly, key proteins in these two pathways, (e.g., FAK [mechano-signaling], and PAR2 and PTK2B [PARs]) were found to be down-regulated in T2D islets which also exhibit elevated PE levels and gain relevance in the context of reduced β cell mass.[2] Moreover, these pathways appeared unique because they have not been associated with other stimulators of β cell proliferation (e.g., inhibitors of DYRK1A, GSK3β, or TGF-β pathways).

The role of PARs signaling in regulating β cell homeostasis has not been explored. The finding that PAR2 is expressed in β cells and that it gets cleaved canonically by trypsin and in a biased fashion by NE,[21,23] suggests that PAR2 signaling, among the PARs, mediates the action of PE. Although we detected trypsin in the islets from T2D donors, the association between low levels of PAR2 and high levels of N-CELA3B in these samples indicates that the activity of PE overcomes the effects of trypsin in regulating PAR2 expression and signaling. Thus, it is likely that PE affects β cell homeostasis by non-canonically cleaving PAR2, disarming the tethered ligand and rendering the receptor unresponsive to canonical mitogenic signals (e.g., trypsin).

The mechano-signaling axis is known to regulate β cell viability.[50,51] FAK loss- and gain-of-function experiments indicate that the action of PE also impacts the integrin signaling in β cells. By employing the innovative Brillouin microscopy, we confirmed that PE treatment modified the cell shape and increased the mechanical stiffness of β cells. These findings are consistent with a loss of cellular integrity and the formation of stress fibers, usually observed upon the induction of the apoptotic program.[52,53] Such changes could be dictated by the effects of PE on interrupting the interactions between β cells and the ECM or modifying the ECM that surrounds the β cells.[54] Indeed, elastases are known to increase ECM stiffness by preferentially digesting soft laminin chains, resulting in a higher proportion of hard fibrotic fibers, such as fibronectin or collagen.[55] In addition, the adhesion of β cells to laminin chains, mainly via β-1 integrin, is fundamental to maintain β cell identity, function, and viability.[56,57] Laminin chains are required to initiate β cell neogenesis from ductal pancreatic progenitor cells.[58] In this context, we observed that telaprevir induced up-regulation of identity genes in β cells, and there was simultaneous down-regulation of exocrine cell-specific pathways in the acinar and ductal cells. Whether the preservation of a physiological pancreatic ECM by inhibiting PE directly regulates exocrine-to-endocrine differentiation warrants further investigation. However, the effects of telaprevir on β cell neogenesis could also occur independently of PE inhibition, as previous data demonstrated the ability of ductal cells to generate endocrine cells in the absence of ACs.[59] Our data identify PE as a novel regulator of mechano-signaling in β cells either directly by disrupting the connections between β cells and the ECM, or indirectly by remodeling the ECM and reducing cell viability.

To study the effect of PE on β cell viability via the mechano-signaling and PAR2 cascade, we simultaneously ablated FAK expression and inhibited PAR2 receptor in βH3 cells. Strikingly, telaprevir reversed the detrimental effect of PE in siFAK-FSSLRY cells but failed to boost β cell viability compared with vehicle-treated samples, as observed in control cells. These results suggest that telaprevir targets yet poorly understood mechanism(s) distinct from the mechano-signaling and PAR2 pathways that are independent of PE inhibition.

In sum, our studies provide insights into the role of PE in regulating the acinar-to-β cell crosstalk by mechano-signaling and the PAR2 signaling pathways to determine β cell viability. The ability of telaprevir, an FDA-approved potent PE inhibitor to improve human β cell survival and proliferation, together with previous reports on its ability to increase circulating C-peptide and to reduce HbA1C levels in HCV-infected individuals with diabetes,[60,61] provides a therapeutic opportunity to expand β cell mass and reverse diabetes in patients. Whether these effects are linked to insulin signaling and resistance in the exocrine pancreas warrants further investigation.

Limitations of the study

Our fundamental observation is the detection of cleaved and active form of CELA3B in the physiological islet microenvironment, and the up-regulation of the CELA3B gene in ACs and cleaved CELA3B protein in islets of subjects with T2D. However, our immunostaining studies presented a few limitations: (1) we used a single section from the head region of the pancreas per donor, therefore further studies are needed to evaluate whether similar expression patterns are maintained in other regions of the human pancreas; (2) the identification of a reliable marker to label endocrine cell membranes represented a challenge. Indeed, we used E-cadherin antibodies to mark cell borders and clarify N-CELA3B localization within the islets. However, the staining appeared to be weaker in endocrine cells than in exocrine cells. That is likely because E-cadherin, as well as other cell junction proteins (e.g., N-cadherin or β-catenin), is expressed at low levels in endocrine cells, originated from a mesodermal lineage.[62] In addition, β cell-specific membrane markers (e.g., GLUT1), abundant in physiological conditions, are down-regulated in T2D,[63] revealing their unsuitability for our studies. Another limitation is represented by the limited effect of telaprevir on glucose tolerance in our DIO models, despite the significant impact on β cell mass. Further investigation using a shorter period of HFD exposure and/or longer treatment with telaprevir will clarify the ability of telaprevir to improve glucose tolerance. Although, we provided mechanistic evidence that telaprevir regulates β cell viability mainly by blocking PE in the islet milieu, as other neutrophil proteases are not expressed in islet preparations, further studies are required to assess the effect of telaprevir on the activity of circulating enzymes, including NE, when administered *in vivo*, and the impact of such inhibition on the regulation of glucose homeostasis.

STAR★METHODS

Detailed methods are provided in the online version of this paper and include the following:

SUPPLEMENTAL INFORMATION

Supplemental information can be found online at https://doi.org/10.1016/j.cmet.2023.05.007.

ACKNOWLEDGMENTS

We thank Jonathan Dreyfuss PhD and Hui Pan PhD (Joslin Bioinformatics and Biostatistics Core) for their assistance with analyzing the phospho-antibody and single-cell RNA-seq outputs. We thank Cristopher Cahill (Joslin Advanced Microscopy Core) for his supervision during the confocal imaging. We thank Angela Wood (Joslin Flow Cytometry Core) for assisting with the flow cytometry experiments and analysis. We thank Sevim Kahraman PhD and Susan Bonner-Weir PhD for scientific discussions. We thank Reema Ahmed BS for her assistance with the humanized mouse studies. This research was performed with the support of the Network for Pancreatic Organ Donors with Diabetes (nPOD; RRID:SCR_014641), a collaborative type 1 diabetes research project supported by JDRF (nPOD: 5-SRA-2018-557-Q-R) and The Leona M. & Harry B. Helmsley Charitable Trust (grant # 2018PG-T1D053, G-2108-04793). The content and views expressed are the responsibility of the authors and do not necessarily reflect the official view of nPOD. Organ Procurement Organizations (OPO) partnering with nPOD to provide research resources are listed at http://www.jdrfnpod.org/for-partners/npod-partners/. Human pancreatic islets were provided by the NIDDK-funded Integrated Islet Distribution Program (IIDP) (RRID:SCR_014387) at City of Hope, NIH grant # 2UC4DK098085.This work was supported by NIH grants R01 DK103215 (R.N.K.), HIRN U01 DK123717 (R.N.K. and B.K.W.), R01 DK122332 (G.G.H.), UC4DK116255 (A.C.), R01 DK113597 (A.C.), and P30 DK 36836 (Joslin DRC); JDRF grant 3-PDF-2020-935-A-N (G.B.), Mary K. Iacocca Junior Postdoctoral Fellowship (D.F.D.J.), ADA Postdoctoral Fellowship 7-20-PDF-140 (D.F.D.J.), and in part by R01 DK067536 (R.N.K.).

AUTHOR CONTRIBUTIONS

G.B. designed the study, performed the experiments, analyzed the data, and wrote the manuscript. A.V. generated the HTS data and assisted with the analysis. J.H. performed the immunostaining and assisted with the analysis. O.I. and Y.Z. maintained animal cohorts and assisted with mouse studies. K.-C.L. performed the zebrafish studies and assisted with the analysis. A.M.E. assisted with performing the Brillouin imaging assays and the analysis. D.F.D.J. and K.F. provided human samples and assisted with the analysis. G.D. contributed to generating the overexpression results. C.A.L. and O.G.C. performed and analyzed the perifusion data. G.G.H. supervised the perifusion experiments and assisted with the analysis. S.-H.Y. supervised the Brillouin microscopy analysis and assisted with the analysis. O.A. supervised the zebrafish studies and assisted with the analysis. A.C. provided reagents and assisted with the analysis. B.K.W. supervised the HTS and scRNA-seq experiments and assisted with the analysis. R.N.K. designed the study, directed the project, and edited the manuscript. All authors edited, read, and approved the final manuscript.

DECLARATION OF INTERESTS

R.N.K. is a member of the Scientific Advisory Board and served as a consultant for Novo Nordisk, Biomea, and Inversago Pharma.

INCLUSION AND DIVERSITY

We support inclusive, diverse, and equitable conduct of research.

Received: November 29, 2021
Revised: January 21, 2023
Accepted: May 17, 2023
Published: July 11, 2023

REFERENCES

1. Bluestone, J.A., Herold, K., and Eisenbarth, G. (2010). Genetics, pathogenesis and clinical interventions in type 1 diabetes. Nature *464*, 1293–1300. https://doi.org/10.1038/nature08933.
2. Butler, A.E., Janson, J., Bonner-Weir, S., Ritzel, R., Rizza, R.A., and Butler, P.C. (2003). β-cell deficit and increased β-cell apoptosis in humans with type 2 diabetes. Diabetes *52*, 102–110. https://doi.org/10.2337/diabetes.52.1.102.
3. Pagliuca, F.W., Millman, J.R., Gürtler, M., Segel, M., Van Dervort, A., Ryu, J.H., Peterson, Q.P., Greiner, D., and Melton, D.A. (2014). Generation of functional human pancreatic β cells in vitro. Cell *159*, 428–439. https://doi.org/10.1016/j.cell.2014.09.040.
4. Nair, G.G., Liu, J.S., Russ, H.A., Tran, S., Saxton, M.S., Chen, R., Juang, C., Li, M.L., Nguyen, V.Q., Giacometti, S., et al. (2019). Recapitulating endocrine cell clustering in culture promotes maturation of human stem-cell-derived β cells. Nat. Cell Biol. *21*, 263–274. https://doi.org/10.1038/s41556-018-0271-4.
5. Bonner-Weir, S. (2000). Perspective: postnatal pancreatic β cell growth. Endocrinology *141*, 1926–1929. https://doi.org/10.1210/endo.141.6.7567.
6. Dirice, E., De Jesus, D.F., Kahraman, S., Basile, G., Ng, R.W.S., El Ouaamari, A., Teo, A.K.K., Bhatt, S., Hu, J., and Kulkarni, R.N. (2019). Human duct cells contribute to β cell compensation in insulin resistance. JCI Insight *4*. 99576. https://doi.org/10.1172/jci.insight.99576.
7. Basile, G., Qadir, M.M.F., Mauvais-Jarvis, F., Vetere, A., Shoba, V., Modell, A.E., Pastori, R.L., Russ, H.A., Wagner, B.K., and Dominguez-Bendala, J. (2022). Emerging diabetes therapies: bringing back the β-cells. Mol. Metab. *60*, 101477. https://doi.org/10.1016/j.molmet.2022.101477.
8. Dirice, E., Walpita, D., Vetere, A., Meier, B.C., Kahraman, S., Hu, J., Dančík, V., Burns, S.M., Gilbert, T.J., Olson, D.E., et al. (2016). Inhibition of DYRK1A stimulates human β-cell proliferation. Diabetes *65*, 1660–1671. https://doi.org/10.2337/db15-1127.
9. Wang, P., Karakose, E., Liu, H., Swartz, E., Ackeifi, C., Zlatanic, V., Wilson, J., González, B.J., Bender, A., Takane, K.K., et al. (2019). Combined inhibition of DYRK1A, SMAD, and trithorax pathways synergizes to induce robust replication in adult human beta cells. Cell Metab. *29*, 638–652.e5. https://doi.org/10.1016/j.cmet.2018.12.005.
10. Shen, W., Taylor, B., Jin, Q., Nguyen-Tran, V., Meeusen, S., Zhang, Y.Q., Kamireddy, A., Swafford, A., Powers, A.F., Walker, J., et al. (2015). Inhibition of DYRK1A and GSK3B induces human β-cell proliferation. Nat. Commun. *6*, 8372. https://doi.org/10.1038/ncomms9372.
11. Dhawan, S., Dirice, E., Kulkarni, R.N., and Bhushan, A. (2016). Inhibition of TGF-β signaling promotes human pancreatic β-cell replication. Diabetes *65*, 1208–1218. https://doi.org/10.2337/db15-1331.
12. Kondegowda, N.G., Fenutria, R., Pollack, I.R., Orthofer, M., Garcia-Ocaña, A., Penninger, J.M., and Vasavada, R.C. (2015). Osteoprotegerin and denosumab stimulate human beta cell proliferation through inhibition of the receptor activator of NF-κB ligand pathway. Cell Metab. *22*, 77–85. https://doi.org/10.1016/j.cmet.2015.05.021.
13. Rosado-Olivieri, E.A., Aigha, I.I., Kenty, J.H., and Melton, D.A. (2020). Identification of a LIF-responsive, replication-competent subpopulation of human β cells. Cell Metab. *31*, 327–338.e6. https://doi.org/10.1016/j.cmet.2019.12.009.
14. El Ouaamari, A., Dirice, E., Gedeon, N., Hu, J., Zhou, J.Y., Shirakawa, J., Hou, L., Goodman, J., Karampelias, C., Qiang, G., et al. (2016). SerpinB1 promotes pancreatic β cell proliferation. Cell Metab. *23*, 194–205. https://doi.org/10.1016/j.cmet.2015.12.001.
15. Dominici, R., and Franzini, C. (2002). Fecal Elastase-1 as a test for pancreatic function: a review. Clin. Chem. Lab. Med. *40*, 325–332. https://doi.org/10.1515/CCLM.2002.051.
16. Ohlsson, K., and Olsson, A.S. (1976). Purification and partial characterization of human pancreatic elastase. Hoppe Seylers Z. Physiol. Chem. *357*, 1153–1161. https://doi.org/10.1515/bchm2.1976.357.2.1153.
17. Hardt, P.D., Krauss, A., Bretz, L., Porsch-Özcürümez, M., Schnell-Kretschmer, H., Mäser, E., Bretzel, R.G., Zekhorn, T., and Klör, H.U. (2000). Pancreatic exocrine function in patients with type 1 and type 2 diabetes mellitus. Acta Diabetol. *37*, 105–110. https://doi.org/10.1007/s005920070011.
18. Esteghamat, F., Broughton, J.S., Smith, E., Cardone, R., Tyagi, T., Guerra, M., Szabó, A., Ugwu, N., Mani, M.V., Azari, B., et al. (2019). CELA2A mutations predispose to early-onset atherosclerosis and metabolic syndrome and affect plasma insulin and platelet activation. Nat. Genet. *51*, 1233–1243. https://doi.org/10.1038/s41588-019-0470-3.
19. Moore, P.C., Cortez, J.T., Chamberlain, C.E., Alba, D., Berger, A.C., Quandt, Z., Chan, A., Cheng, M.H., Bautista, J.L., Peng, J., et al. (2019). Elastase 3B mutation links to familial pancreatitis with diabetes and pancreatic adenocarcinoma. J. Clin. Invest. *129*, 4676–4681. https://doi.org/10.1172/JCI129961.
20. Chua, F., and Laurent, G.J. (2006). Neutrophil elastase: mediator of extracellular matrix destruction and accumulation. Proc. Am. Thorac. Soc. *3*, 424–427. https://doi.org/10.1513/pats.200603-078AW.
21. Ramachandran, R., Mihara, K., Chung, H., Renaux, B., Lau, C.S., Muruve, D.A., DeFea, K.A., Bouvier, M., and Hollenberg, M.D. (2011). Neutrophil elastase acts as a biased agonist for proteinase-activated receptor-2 (PAR2). J. Biol. Chem. *286*, 24638–24648. https://doi.org/10.1074/jbc.M110.201988.
22. Hänzelmann, S., Wang, J., Güney, E., Tang, Y., Zhang, E., Axelsson, A.S., Nenonen, H., Salehi, A.S., Wollheim, C.B., Zetterberg, E., et al. (2015). Thrombin stimulates insulin secretion via protease-activated receptor-3. Islets *7*. e1118195. https://doi.org/10.1080/19382014.2015.1118195.
23. Regard, J.B., Kataoka, H., Cano, D.A., Camerer, E., Yin, L., Zheng, Y.W., Scanlan, T.S., Hebrok, M., and Coughlin, S.R. (2007). Probing cell type–specific functions of Gi in vivo identifies GPCR regulators of insulin secretion. J. Clin. Invest. *117*, 4034–4043. https://doi.org/10.1172/JCI32994.
24. Benazra, M., Lecomte, M.J., Colace, C., Müller, A., Machado, C., Pechberty, S., Bricout-Neveu, E., Grenier-Godard, M., Solimena, M., Scharfmann, R., et al. (2015). A human beta cell line with drug inducible excision of immortalizing transgenes. Mol. Metab. *4*, 916–925. https://doi.org/10.1016/j.molmet.2015.09.008.

25. Stoffers, D.A., Zinkin, N.T., Stanojevic, V., Clarke, W.L., and Habener, J.F. (1997). Pancreatic agenesis attributable to a single nucleotide deletion in the human IPF1 gene coding sequence. Nat. Genet. *15*, 106–110. https://doi.org/10.1038/ng0197-106.

26. Chen, C., Li, X., Neumann, C.S., Lo, M.M., and Schreiber, S.L. (2005). Convergent diversity-oriented synthesis of small-molecule hybrids. Angew. Chem. Int. Ed. Engl. *44*, 2249–2252. https://doi.org/10.1002/anie.200462798.

27. Corsello, S.M., Bittker, J.A., Liu, Z., Gould, J., McCarren, P., Hirschman, J.E., Johnston, S.E., Vrcic, A., Wong, B., Khan, M., et al. (2017). The Drug Repurposing Hub: a next-generation drug library and information resource. Nat. Med. *23*, 405–408. https://doi.org/10.1038/nm.4306.

28. Tan, D.S. (2005). Diversity-oriented synthesis: exploring the intersections between chemistry and biology. Nat. Chem. Biol. *1*, 74–84. https://doi.org/10.1038/nchembio0705-74.

29. Wawer, M.J., Li, K., Gustafsdottir, S.M., Ljosa, V., Bodycombe, N.E., Marton, M.A., Sokolnicki, K.L., Bray, M.A., Kemp, M.M., Winchester, E., et al. (2014). Toward performance-diverse small-molecule libraries for cell-based phenotypic screening using multiplexed high-dimensional profiling. Proc. Natl. Acad. Sci. USA *111*, 10911–10916. https://doi.org/10.1073/pnas.1410933111.

30. Kawabata, K., Suzuki, M., Sugitani, M., Imaki, K., Toda, M., and Miyamoto, T. (1991). ONO-5046, a novel inhibitor of human neutrophil elastase. Biochem. Biophys. Res. Commun. *177*, 814–820. https://doi.org/10.1016/0006-291X(91)91862-7.

31. Greiner, D.L., Brehm, M.A., Hosur, V., Harlan, D.M., Powers, A.C., and Shultz, L.D. (2011). Humanized mice for the study of type 1 and type 2 diabetes. Ann. N. Y. Acad. Sci. *1245*, 55–58. https://doi.org/10.1111/j.1749-6632.2011.06318.x.

32. Curado, S., Anderson, R.M., Jungblut, B., Mumm, J., Schroeter, E., and Stainier, D.Y.R. (2007). Conditional targeted cell ablation in zebrafish: A new tool for regeneration studies. Dev. Dyn. *236*, 1025–1035. https://doi.org/10.1002/dvdy.21100.

33. Lu, J., Liu, K.C., Schulz, N., Karampelias, C., Charbord, J., Hilding, A., Rautio, L., Bertolino, P., Östenson, C.G., Brismar, K., et al. (2016). IGFBP1 increases β-cell regeneration by promoting α- to β-cell transdifferentiation. EMBO J. *35*, 2026–2044. https://doi.org/10.15252/embj.201592903.

34. Zhao, P., Lieu, T., Barlow, N., Sostegni, S., Haerteis, S., Korbmacher, C., Liedtke, W., Jimenez-Vargas, N.N., Vanner, S.J., and Bunnett, N.W. (2015). Neutrophil elastase activates protease-activated Receptor-2 (PAR2) and transient receptor potential vanilloid 4 (TRPV4) to cause inflammation and pain. J. Biol. Chem. *290*, 13875–13887. https://doi.org/10.1074/jbc.M115.642736.

35. DeFea, K.A., Zalevsky, J., Thoma, M.S., Déry, O., Mullins, R.D., and Bunnett, N.W. (2000). β-arrestin–dependent Endocytosis of proteinase-activated Receptor 2 Is Required for intracellular Targeting of activated ERK1/2. J. Cell Biol. *148*, 1267–1281.

36. Kahraman, S., Manna, D., Dirice, E., Maji, B., Small, J., Wagner, B.K., Choudhary, A., and Kulkarni, R.N. (2021). Harnessing reaction-based probes to preferentially target pancreatic β-cells and β-like cells. Life Sci. Alliance *4*. e202000840. https://doi.org/10.26508/lsa.202000840.

37. Lee, M., Maji, B., Manna, D., Kahraman, S., Elgamal, R.M., Small, J., Kokkonda, P., Vetere, A., Goldberg, J.M., Lippard, S.J., et al. (2020). Native zinc catalyzes selective and traceless release of small molecules in β-cells. J. Am. Chem. Soc. *142*, 6477–6482. https://doi.org/10.1021/jacs.0c00099.

38. Sells, M.A., Knaus, U.G., Bagrodia, S., Ambrose, D.M., Bokoch, G.M., and Chernoff, J. (1997). Human p21-activated kinase (Pak1) regulates actin organization in mammalian cells. Curr. Biol. *7*, 202–210. https://doi.org/10.1016/S0960-9822(97)70091-5.

39. Prevedel, R., Diz-Muñoz, A., Ruocco, G., and Antonacci, G. (2019). Brillouin microscopy: an emerging tool for mechanobiology. Nat. Methods *16*, 969–977. https://doi.org/10.1038/s41592-019-0543-3.

40. Logsdon, C.D., and Ji, B. (2013). The role of protein synthesis and digestive enzymes in acinar cell injury. Nat. Rev. Gastroenterol. Hepatol. *10*, 362–370. https://doi.org/10.1038/nrgastro.2013.36.

41. Aida, K., Saitoh, S., Nishida, Y., Yokota, S., Ohno, S., Mao, X., Akiyama, D., Tanaka, S., Awata, T., Shimada, A., et al. (2014). Distinct cell clusters touching islet cells induce islet cell replication in association with overexpression of regenerating gene (REG) protein in fulminant Type 1 diabetes. PLoS One *9*. e95110. https://doi.org/10.1371/journal.pone.0095110.

42. Egozi, A., Bahar Halpern, K.B., Farack, L., Rotem, H., and Itzkovitz, S. (2020). Zonation of pancreatic acinar cells in diabetic mice. Cell Rep. *32*, 108043. https://doi.org/10.1016/j.celrep.2020.108043.

43. Kahraman, S., Dirice, E., Basile, G., Diegisser, D., Alam, J., Johansson, B.B., Gupta, M.K., Hu, J., Huang, L., Soh, C.L., et al. (2022). Abnormal exocrine–endocrine cell cross-talk promotes β-cell dysfunction and loss in MODY8. Nat. Metab. *4*, 76–89. https://doi.org/10.1038/s42255-021-00516-2.

44. Ræder, H., McAllister, F.E., Tjora, E., Bhatt, S., Haldorsen, I., Hu, J., Willems, S.M., Vesterhus, M., El Ouaamari, A., Liu, M., et al. (2014). Carboxyl-ester lipase maturity-onset diabetes of the young is associated with development of pancreatic cysts and upregulated MAPK signaling in secretin-stimulated duodenal fluid. Diabetes *63*, 259–269. https://doi.org/10.2337/db13-1012.

45. Cinti, F., Bouchi, R., Kim-Muller, J.Y., Ohmura, Y., Sandoval, P.R., Masini, M., Marselli, L., Suleiman, M., Ratner, L.E., Marchetti, P., et al. (2016). Evidence of β-cell dedifferentiation in human Type 2 diabetes. J. Clin. Endocrinol. Metab. *101*, 1044–1054. https://doi.org/10.1210/jc.2015-2860.

46. Lawlor, N., George, J., Bolisetty, M., Kursawe, R., Sun, L., Sivakamasundari, V., Kycia, I., Robson, P., and Stitzel, M.L. (2017). Single-cell transcriptomes identify human islet cell signatures and reveal cell-type-specific expression changes in type 2 diabetes. Genome Res. *27*, 208–222. https://doi.org/10.1101/gr.212720.116.

47. Segerstolpe, A., Palasantza, A., Eliasson, P., Andersson, E.M., Andréasson, A.C., Sun, X., Picelli, S., Sabirsh, A., Clausen, M., Bjursell, M.K., et al. (2016). Single-cell transcriptome profiling of human pancreatic islets in health and type 2 diabetes. Cell Metab. *24*, 593–607. https://doi.org/10.1016/j.cmet.2016.08.020.

48. Xin, Y., Kim, J., Okamoto, H., Ni, M., Wei, Y., Adler, C., Murphy, A.J., Yancopoulos, G.D., Lin, C., and Gromada, J. (2016). RNA sequencing of single human islet cells reveals Type 2 diabetes genes. Cell Metab. *24*, 608–615. https://doi.org/10.1016/j.cmet.2016.08.018.

49. Puri, S., Roy, N., Russ, H.A., Leonhardt, L., French, E.K., Roy, R., Bengtsson, H., Scott, D.K., Stewart, A.F., and Hebrok, M. (2018). Replication confers β cell immaturity. Nat. Commun. *9*, 485. https://doi.org/10.1038/s41467-018-02939-0.

50. Diaferia, G.R., Jimenez-Caliani, A.J., Ranjitkar, P., Yang, W., Hardiman, G., Rhodes, C.J., Crisa, L., and Cirulli, V. (2013). β1 integrin is a crucial regulator of pancreatic β-cell expansion. Development *140*, 3360–3372. https://doi.org/10.1242/dev.098533.

51. Cai, E.P., Casimir, M., Schroer, S.A., Luk, C.T., Shi, S.Y., Choi, D., Dai, X.Q., Hajmrle, C., Spigelman, A.F., Zhu, D., et al. (2012). In vivo role of focal adhesion kinase in regulating pancreatic β-cell mass and function through insulin signaling, actin dynamics, and granule trafficking. Diabetes *61*, 1708–1718. https://doi.org/10.2337/db11-1344.

52. Hessler, J.A., Budor, A., Putchakayala, K., Mecke, A., Rieger, D., Banaszak Holl, M.M., Orr, B.G., Bielinska, A., Beals, J., and Baker, J. (2005). Atomic force microscopy study of early morphological changes during apoptosis. Langmuir *21*, 9280–9286. https://doi.org/10.1021/la051837g.

53. Islam, M., Mezencev, R., McFarland, B., Brink, H., Campbell, B., Tasadduq, B., Waller, E.K., Lam, W., Alexeev, A., and Sulchek, T. (2018). Microfluidic cell sorting by stiffness to examine heterogenic responses of cancer cells to chemotherapy. Cell Death Dis. *9*, 239. https://doi.org/10.1038/s41419-018-0266-x.

54. Discher, D.E., Janmey, P., and Wang, Y.L. (2005). Tissue cells feel and respond to the stiffness of their substrate. Science *310*, 1139–1143. https://doi.org/10.1126/science.1116995.

55. Shiokawa, M., Kodama, Y., Sekiguchi, K., Kuwada, T., Tomono, T., Kuriyama, K., Yamazaki, H., Morita, T., Marui, S., Sogabe, Y., et al. (2018). Laminin 511 is a target antigen in autoimmune pancreatitis. Sci. Transl. Med. *10*. eaaq0997. https://doi.org/10.1126/scitranslmed.aaq0997.

56. Jiang, F.X., Georges-Labouesse, E., and Harrison, L.C. (2001). Regulation of laminin 1-induced pancreatic beta-cell differentiation by alpha6 integrin and alpha-dystroglycan. Mol. Med. Camb. Mass. *7*, 107–114.

57. Weber, L.M., Hayda, K.N., and Anseth, K.S. (2008). Cell-matrix interactions improve beta-cell survival and insulin secretion in three-dimensional culture. Tissue Eng. Part A *14*, 1959–1968. https://doi.org/10.1089/ten.tea.2007.0238.

58. Mamidi, A., Prawiro, C., Seymour, P.A., de Lichtenberg, K.H., Jackson, A., Serup, P., and Semb, H. (2018). Mechanosignalling via integrins directs fate decisions of pancreatic progenitors. Nature *564*, 114–118. https://doi.org/10.1038/s41586-018-0762-2.

59. Criscimanna, A., Speicher, J.A., Houshmand, G., Shiota, C., Prasadan, K., Ji, B., Logsdon, C.D., Gittes, G.K., and Esni, F. (2011). Duct cells contribute to regeneration of endocrine and acinar cells following pancreatic damage in adult mice. Gastroenterology *141*, 1451–1462. https://doi.org/10.1053/j.gastro.2011.07.003.

60. Davis, T.M.E., Davis, W.A., and Jeffrey, G. (2017). Successful withdrawal of insulin therapy after post-treatment clearance of hepatitis C virus in a man with Type 2 diabetes. Am. J. Case Rep. *18*, 414–417. https://doi.org/10.12659/ajcr.903600.

61. Tallón de Lara, P., Himschoot, T., Frossard, J.L., and Negro, F. (2014). Does telaprevir possess a direct antidiabetic effect? Liver Int. *34*, 967–969. https://doi.org/10.1111/liv.12440.

62. Liu, K.C., Villasenor, A., Bertuzzi, M., Schmitner, N., Radros, N., Rautio, L., Mattonet, K., Matsuoka, R.L., Reischauer, S., Stainier, D.Y., et al. (2021). Insulin-producing β-cells regenerate ectopically from a mesodermal origin under the perturbation of hemato-endothelial specification. eLife *10*. e65758. https://doi.org/10.7554/eLife.65758.

63. Del Guerra, S., Lupi, R., Marselli, L., Masini, M., Bugliani, M., Sbrana, S., Torri, S., Pollera, M., Boggi, U., Mosca, F., et al. (2005). Functional and molecular defects of pancreatic islets in human Type 2 diabetes. Diabetes *54*, 727–735. https://doi.org/10.2337/diabetes.54.3.727.

64. Andersson, O., Adams, B.A., Yoo, D., Ellis, G.C., Gut, P., Anderson, R.M., German, M.S., and Stainier, D.Y.R. (2012). Adenosine signaling promotes regeneration of pancreatic β cells in vivo. Cell Metab. *15*, 885–894. https://doi.org/10.1016/j.cmet.2012.04.018.

65. Ninov, N., Borius, M., and Stainier, D.Y.R. (2012). Different levels of Notch signaling regulate quiescence, renewal and differentiation in pancreatic endocrine progenitors. Development *139*, 1557–1567. https://doi.org/10.1242/dev.076000.

66. Ritchie, M.E., Phipson, B., Wu, D., Hu, Y., Law, C.W., Shi, W., and Smyth, G.K. (2015). limma powers differential expression analyses for RNA-sequencing and microarray studies. Nucleic Acids Res. *43*. e47. https://doi.org/10.1093/nar/gkv007.

67. Robinson, M.D., McCarthy, D.J., and Smyth, G.K. (2010). edgeR: a Bioconductor package for differential expression analysis of digital gene expression data. Bioinform. Oxf. Engl. *26*, 139–140. https://doi.org/10.1093/bioinformatics/btp616.

68. Bankhead, P., Loughrey, M.B., Fernández, J.A., Dombrowski, Y., McArt, D.G., Dunne, P.D., McQuaid, S., Gray, R.T., Murray, L.J., Coleman, H.G., et al. (2017). QuPath: open source software for digital pathology image analysis. Sci. Rep. *7*, 16878. https://doi.org/10.1038/s41598-017-17204-5.

69. De Jesus, D.F., Zhang, Z., Kahraman, S., Brown, N.K., Chen, M., Hu, J., Gupta, M.K., He, C., and Kulkarni, R.N. (2019). m(6)A mRNA methylation regulates human β-cell biology in physiological states and in type 2 diabetes. Nat. Metab. *1*, 765–774. https://doi.org/10.1038/s42255-019-0089-9.

70. Pisharath, H., Rhee, J.M., Swanson, M.A., Leach, S.D., and Parsons, M.J. (2007). Targeted ablation of beta cells in the embryonic zebrafish pancreas using E. coli nitroreductase. Mech. Dev. *124*, 218–229. https://doi.org/10.1016/j.mod.2006.11.005.

71. Watanabe, T., Yaegashi, H., Koizumi, M., Toyota, T., and Takahashi, T. (1997). The lobular architecture of the normal human pancreas: a computer-assisted three-dimensional reconstruction study. Pancreas *15*, 48–52.

72. Pisania, A., Weir, G.C., O'Neil, J.J., Omer, A., Tchipashvili, V., Lei, J., Colton, C.K., and Bonner-Weir, S. (2010). Quantitative analysis of cell composition and purity of human pancreatic islet preparations. Lab. Invest. *90*, 1661–1675. https://doi.org/10.1038/labinvest.2010.124.

73. Cabrera, O., Berman, D.M., Kenyon, N.S., Ricordi, C., Berggren, P.O., and Caicedo, A. (2006). The unique cytoarchitecture of human pancreatic islets has implications for islet cell function. Proc. Natl. Acad. Sci. USA *103*, 2334–2339. https://doi.org/10.1073/pnas.0510790103.

74. Wirjanata, G., Handayuni, I., Zaloumis, S.G., Chalfein, F., Prayoga, P., Kenangalem, E., Poespoprodjo, J.R., Noviyanti, R., Simpson, J.A., Price, R.N., et al. (2016). Analysis of ex vivo drug response data of Plasmodium clinical isolates: the pros and cons of different computer programs and online platforms. Malar. J. *15*, 137. https://doi.org/10.1186/s12936-016-1173-1.

75. McCarthy, D.J., Campbell, K.R., Lun, A.T.L., and Wills, Q.F. (2017). Scater: pre-processing, quality control, normalization and visualization of single-cell RNA-seq data in R. Bioinform. Oxf. Engl. *33*, 1179–1186. https://doi.org/10.1093/bioinformatics/btw777.

76. Lun, A.T.L., Bach, K., and Marioni, J.C. (2016). Pooling across cells to normalize single-cell RNA sequencing data with many zero counts. Genome Biol. *17*, 75. https://doi.org/10.1186/s13059-016-0947-7.

77. Muraro, M.J., Dharmadhikari, G., Grün, D., Groen, N., Dielen, T., Jansen, E., van Gurp, L., Engelse, M.A., Carlotti, F., de Koning, E.J.P., et al. (2016). A single-cell transcriptome atlas of the human pancreas. Cell Syst. *3*, 385–394.e3. https://doi.org/10.1016/j.cels.2016.09.002.

78. Wu, D., Lim, E., Vaillant, F., Asselin-Labat, M.L., Visvader, J.E., and Smyth, G.K. (2010). ROAST: rotation gene set tests for complex microarray experiments. Bioinform. Oxf. Engl. *26*, 2176–2182. https://doi.org/10.1093/bioinformatics/btq401.

79. Cheadle, C., Vawter, M.P., Freed, W.J., and Becker, K.G. (2003). Analysis of microarray data using Z score transformation. J. Mol. Diagn. *5*, 73–81. https://doi.org/10.1016/S1525-1578(10)60455-2.

80. Subramanian, A., Tamayo, P., Mootha, V.K., Mukherjee, S., Ebert, B.L., Gillette, M.A., Paulovich, A., Pomeroy, S.L., Golub, T.R., Lander, E.S., et al. (2005). Gene set enrichment analysis: a knowledge-based approach for interpreting genome-wide expression profiles. Proc. Natl. Acad. Sci. USA *102*, 15545–15550. https://doi.org/10.1073/pnas.0506580102.

81. Liberzon, A., Birger, C., Thorvaldsdóttir, H., Ghandi, M., Mesirov, J.P., and Tamayo, P. (2015). The molecular signatures database (MSigDB) hallmark gene set collection. Cell Syst. *1*, 417–425. https://doi.org/10.1016/j.cels.2015.12.004.

82. Scarcelli, G., and Yun, S.H. (2007). Confocal Brillouin microscopy for three-dimensional mechanical imaging. Nat. Photonics *2*, 39–43. https://doi.org/10.1038/nphoton.2007.250.

83. Eltony, A.M., Shao, P., and Yun, S.H. (2022). Measuring mechanical anisotropy of the cornea with Brillouin microscopy. Nat. Commun. *13*, 1354. https://doi.org/10.1038/s41467-022-29038-5.

84. Shao, P., Eltony, A.M., Seiler, T.G., Tavakol, B., Pineda, R., Koller, T., Seiler, T., and Yun, S.H. (2019). Spatially-resolved Brillouin spectroscopy reveals biomechanical abnormalities in mild to advanced keratoconus in vivo. Sci. Rep. *9*, 7467. https://doi.org/10.1038/s41598-019-43811-5.

85. Li, C.H., and Tam, P.K.S. (1998). An iterative algorithm for minimum cross entropy thresholding. Pattern Recognit. Lett. *19*, 771–776. https://doi.org/10.1016/S0167-8655(98)00057-9.

Please cite this article in press as: Basile et al., Excess pancreatic elastase alters acinar-β cell communication by impairing the mechano-signaling and the PAR2 pathways, Cell Metabolism (2023), https://doi.org/10.1016/j.cmet.2023.05.007

STAR★METHODS

KEY RESOURCES TABLE

REAGENT or RESOURCE	SOURCE	IDENTIFIER
Antibodies		
Guinea pig polyclonal anti-Insulin	Abcam	Cat# ab7842; RRID: AB_306130
Purified Mouse monoclonal anti-Ki67 (clone B56)	BD Biosciences	Cat# 550609; RRID: AB_393778
Rabbit polyclonal anti-phopho-Histone H3 (Ser10)	Millipore	Cat# 06-570; RRID: AB_310177
Mouse monoclonal anti-Elastase 3A (clone 14-3)	Santa Cruz Biotechnology	Cat# sc-100527; RRID: AB_628381
Rabbit polyclonal anti-CELA3B(N-terminal)	Sigma	Cat# SAB1306246
Mouse monoclonal anti-E-Cadherin (clone 4A2)	Cell Signaling Technology	Cat# 14472; RRID: AB_2728770
Recombinant Rabbit monoclonal anti-glucagon (clone EP3070)	Abcam	Cat# ab92517; RRID: AB_10561971
Mouse monoclonal anti-ELA3B (clone 3H3)	Sigma	Cat# SAB1409028;
Mouse monoclonal anti-trypsin (clone D-1)	Santa Cruz Biotechnology	Cat# sc-137077, RRID:AB_2300318
Mouse monoclonal anti-Amylase	Santa Cruz Biotechnology	Cat# sc-46657, RRID:AB_626668
Rabbit monoclonal anti-PDX1 (D59H3)	Cell Signaling Technology	Cat# 5679; RRID: AB_10706174
Mouse monoclonal anti-PAR2 (SAM11)	Thermo Fisher	Cat# 35-2300; RRID: AB_2533199
Mouse monoclonal anti-PAR3 (G-4)	Santa Cruz Biotechnology	Cat# sc-393127
Rabbit polyclonal anti-FAK	Cell Signaling Technology	Cat# 3285; RRID: AB_2269034
Rabbit polyclonal anti-phopsho PAK1 (Ser144)/PAK2 (Ser141)	Cell Signaling Technology	Cat# 2606; RRID: AB_2299279
Rabbit polyclonal anti-PAK1/2/3	Cell Signaling Technology	Cat# 2604; RRID: AB_2160225
Rabbit polyclonal anti-phopsho p44/42 MAPK (Erk 1/2) (Thr202/Tyr204)	Cell Signaling Technology	Cat# 9101; RRID: AB_331646
Rabbit polyclonal anti-p44/42 MAPK (Erk 1/2)	Cell Signaling Technology	Cat# 9102; RRID: AB_320744
Rabbit monoclonal anti-β-actin (13E5)	Cell Signaling Technology	Cat# 4970; RRID: AB_2223172
Mouse monoclonal anti-Vinculin (7F9)	Santa Cruz Biotechnology	Cat# sc-73614; RRID: AB_1131294
Rabbit monoclonal anti-GAPDH (D16H11)	Cell Signaling Technology	Cat# 5174; RRID: AB_10622025
APC Annexin V	BD Biosciences	Cat# 550474; RRID: AB_2868885
Biological samples		
Human islets	IIDP/Prodo Labs	Table S1
Human acinar cells	Prodo Labs	
Human ductal cells	Prodo Labs	
Human pancreatic sections	nPOD	
Human bone marrow Total RNA	Takara	Cat# 636591
Chemicals, peptides, and recombinant proteins		
TRIzol Reagent	Thermo Fisher	Cat# 15596018
Pierce RIPA buffer	Thermo Fisher	Cat# 89901
Performer Set	Broad Institute	Wawer et al.[29]
Informer Set	Broad Institute	Chen et al.[26]; Tan[28]
Repurpose Set	Broad Institute	Corsello et al.[27]
Telaprevir	Selleckchem	Cat# S1538

(*Continued on next page*)

Please cite this article in press as: Basile et al., Excess pancreatic elastase alters acinar-β cell communication by impairing the mechano-signaling and the PAR2 pathways, Cell Metabolism (2023), https://doi.org/10.1016/j.cmet.2023.05.007

Continued

REAGENT or RESOURCE	SOURCE	IDENTIFIER
Sivelestat	Selleckchem	Cat# S4666
Tebipenem Pivoxil	Selleckchem	Cat# S2159
Human pancreatic elastase	Elastin Product Company	Cat# HE145
Porcine pancreatic elastase	Elastin Product Company	Cat# ES438
Human neutrophil elastase	Elastin Product Company	Cat# SE563
Human cathepsin G	Elastin Product Company	Cat# SG623
N-Methoxysuccinyl-Ala-Ala-Pro-Val p-nitroanilide	Sigma	Cat# M4765
N-Succinyl-Ala-Ala-Pro-Phe p-nitroanilide	Elastin Product Company	Cat# SG554
FSSLRY-NH_2	Tocris	Cat# 4751
4-Hydroxytamoxifen (4-OHT)	Sigma	Cat# H6278
Elastase 3B (ELA3B) recombinant protein	MyBioSource	Cat# MBS2012053
DA-ZP1	From Dr. Amit Choudhary	Lee et al.[37]
Critical commercial assays		
Caspase-3/CPP32 Colorimetric assay kit	Biovision	Cat# K106
Click-iT Plus EdU Alexa Fluor™ 488 Flow Cytometry Assay Kit	Thermo Fisher	Cat# C10632
Click-iT Plus EdU Alexa Fluor™ 647 Flow Cytometry Assay Kit	Thermo Fisher	Cat# C10634
eBioscience Annexin V Apoptosis Detection Kit APC	Thermo Fisher	Cat# 88-8007-72
ApopTag Fluorescein In Situ Apoptosis Detection Kit	Sigma	Cat# S7110
EnzCheck Elastase Assay kit	Thermo Fisher	Cat# E-12056
Phopsho-antibody microarray	Kinexus	Cat# KAM-1325
Chromium Single Cell 3' Library & Gel Bead Kit v2	10x Genomics	Cat# PN-120237
Chromium Single Cell A Chip Kit	10x Genomics	Cat# PN-120236
Chromium i7 Sample index plate	10x Genomics	Cat# PN-220103
Dead cell removal kit	Miltenyi Biotec	Cat# 130-090-101
Insulin Human ELISA kit	Mercodia	Cat# 10-1113-01
C-peptide Human ELISA kit	Mercodia	Cat# 10-1136-01
Mouse C-peptide ELISA kit	Crystal Chem	Cat# 90050
Deposited data		
Single-cell RNA-seq dataset	This paper	GSE190447
Phospho-antibody microarray dataset	This paper	GSE189986
Experimental models: Cell lines		
EndoC-βH1	Human Cell Design	RRID: CVCL-L909
EndoC-βH3	Human Cell Design	RRID: CVCL-IS72
Experimental models: Organisms/strains		
Tg(ins:FLAG-NTR,cryaa:mCherry)^{s950}	From Dr. Olov Andersson	Andersson et al.[64]
Tg(EPV.Tp1-Mmu.Hbb:hist2h2l-mCherry)^{s939}	From Dr. Olov Andersson	Ninov et al.[65]
Tg(ins:flag-NTR);Tg(tp1:H2BmCherry)	From Dr. Olov Andersson	Lu et al.[33]
C57BL/6J	Jackon lab	Cat#:000664 RRID:IMSR_JAX:000664
NOD.Cg-Prkdcscid Il2rgtm1Wjl/SzJ	Jackson lab	Cat#:005557 RRID:IMSR_JAX:005557
Oligonucleotides		
RT-PCT oligonucleotides	IDT	Table S2
ON-TARGETplus Human PTK2 siRNA pool	Dharmacon	Cat# L-003164-00-0010

(*Continued on next page*)

Please cite this article in press as: Basile et al., Excess pancreatic elastase alters acinar-β cell communication by impairing the mechano-signaling and the PAR2 pathways, Cell Metabolism (2023), https://doi.org/10.1016/j.cmet.2023.05.007

Continued

REAGENT or RESOURCE	SOURCE	IDENTIFIER
ON-TARGETplus Non-targeting siRNA pool	Dharmacon	Cat# D-001810-10-20
Recombinant DNA		
pReceiver-M35	Genecopoeia	Cat# EX-NEG-M35-B
ORF Clone PTK2	Genecopoeia	Cat# EX-I0314-M35-B; NM_153831.3
Software and algorithms		
Cellranger version 6.0.0	10x Genomics	https://support.10xgenomics.com/single-cell-gene-expression/software/downloads/latest; RRID:SCR_017344
Differential gene expression analysis of microarrays: limma	https://bioconductor.org/packages/release/; Ritchie et al.[66]	RRID:SCR_010943
Differential gene expression analysis of RNAseq: edgeR	https://bioconductor.org/packages/release/; Robinson et al.[67]	RRID:SCR_012802
ImageJ	http://imagej.net/Contributors;	RRID: SCR_003070
QuPath	https://qupath.github.io; Bankhead et al.[68]	RRID:SCR_018257
GraphPad Prism v9.5.1	www.graphpad.com/	RRID:SCR_002798
Scater	https://bioconductor.org/packages/release/bioc/html/scater.html	RRID:SCR_015954
Other		
RNeasy Mini Kit	Qiagen	Cat# 74106
Lipofectamine 3000 Transfection reagent	Invitrogen	Cat# L3000001
Lipofectamine RNAiMax Transfection reagent	Invitrogen	Cat# 13778075
Annexin V Binding Buffer, 10X concentrate	BD Biosciences	Cat# 556454
Bio-Gel P-4 Gel	Bio-Rad	Cat# 1504124
Osmotic mini pumps	Alzet	Cat# 1004
High-Capacity cDNA Reverse Transcription Kit	Applied Biosystems	Cat# 4368814
Low Fat Diet (10%)	Research Diet	Cat# D12450K
High Fat Diet (60%)	Research Diet	Cat# D12492

RESOURCE AVAILABILITY

Lead Contact

Further information and requests for resources and reagents should be directed to and will be fulfilled by the lead contact, Rohit N. Kulkarni (rohit.kulkarni@joslin.harvard.edu).

Materials availability

This study did not generate new unique reagents

Data and code availability

All data reported in this paper will be shared by the lead contact upon request. Source data and Western blot images for the figures in the manuscript are available as Data S1–Source Data.

The single-cell RNA-sequencing and the phopsho-antibody microarray data were uploaded in the Gene Expression Omnibus (GEO) database and are publicly available as the date of publication with the accession numbers GSE190447 and GSE189986 respectively.

Please cite this article in press as: Basile et al., Excess pancreatic elastase alters acinar-β cell communication by impairing the mechano-signaling and the PAR2 pathways, Cell Metabolism (2023), https://doi.org/10.1016/j.cmet.2023.05.007

EXPERIMENTAL MODEL AND SUBJECT DETAILS

Human exocrine cells and islets

Human acinar cells, ductal cells and islets isolated from non-diabetic (ND) donors or donors with type 2 diabetes (T2D) were obtained from the Integrated Islet Distribution Program (IIDP) or Prodo Laboratories (Table S1). All studies and used protocols were approved by the Joslin Diabetes Center's Committee on Human Studies (CHS#5-05).

Human Pancreas

Human sections from the head region of pancreas of non-diabetic (ND) donors or donors with type 2 diabetes (T2D) were obtained from the nPOD repository (Table S1). CELA3A and N-CELA3B (cleaved and active form) expression was analyzed by immunofluorescence (see below).

Mouse models

C57BL6/J and NSG mice were used for the dietary and human islet transplantation studies respectively. All animals were housed in the pathogen-free Animal Care Facilities at Joslin Diabetes Center, Boston, MA. Studies conducted and protocols used were approved by the Institutional Animal Care and Use Committees of the Joslin Diabetes Center (IACUC #05-01, #2012-09) and were in accordance with National Institute of Health guidelines.

Zebrafish models

All studies involving zebrafish (*Danio rerio*) were performed in accordance with local guidelines and regulations and approved by Stockholm ethical committee (6848-2020). Two previously published transgenic fish lines, including *Tg(ins:FLAG-NTR,cryaa:mCherry)*^{s950} abbreviated as *Tg(ins:flag-NTRzp*[64] and *Tg(EPV.Tp1-Mmu.Hbb:hist2h2l-mCherry)*^{s939} abbreviated as *Tg(tp1:H2BmCherry)*,[65] were crossed to generate *Tg(ins:flag-NTR);Tg(tp1:H2BmCherry)* zebrafish.

METHOD DETAILS

Human pancreatic cell culture

Upon receipt, human islets were cultured overnight (ON) in Miami Media #1A (Cellgro) at 37°C with 5% CO_2, before being processed for the studies listed below, whereas human acinar cells and ductal cells were incubated in RPMI Media (Gibco). For the PE expression studies, 200 human islet equivalents (IEQs), 500 acinar cell clusters, and 100 ductal cell aggregates were collected after ON incubation, washed twice in Dulbecco's phosphate-buffered saline (DPBS, Gibco), and incubated in RIPA buffer (Thermo Fisher) for 15 min to isolate total proteins, or in TRIzol (Invitrogen) for isolating RNA (see below). For the proliferation assays and the high-throughput studies, human islets were starved in Final Wash/Culture Media (Cellgro) for 3 h before being stimulated with Miami Media #1A supplemented with either DMSO (at 1% v/v dilution) or small molecules at the indicated concentrations. For immunohistochemistry studies, 200 hand-picked IEQs were collected after 24 h stimulation, washed twice in DPBS, fixed in 4% paraformaldehyde (PFA, Wako), and embedded in 1% low melting agarose (National Diagnostic). Paraffin sections were analyzed using immunofluorescence procedures (see below). For the phospho-antibody microarray studies, 200 hand-picked IEQs were collected after 10- or 30-min stimulation and processed as described below. For the single-cell RNA-Seq (scRNA-Seq) studies, 500 hand-picked IEQs were harvested after 24 h stimulation and processed as described below.

Human islet transplantations

For the human islet transplantation studies, 1000 human IEQs were hand-picked after ON incubation, washed with saline solution and transplanted under the kidney capsule of male 8-to-10-week-old non-obese diabetic-severe combined immunodeficiency-IL2rγ^{null} (NSG)[31] mice as previously described.[6] After 17 days post-transplantation, either DMSO or telaprevir at the indicated concentrations were administrated to mice using osmotic pumps (Alzet, CA) for 28 days as previously described.[14] At the end of the treatment period, human islet grafts and endogenous pancreas were rapidly dissected, fixed in zinc formalin fixative (Z-FIX, Fisher Scientific) overnight at 4°C, and processed for generating 5-μm-thick paraffin-embedded serial sections. Human β-cell viability was assessed by immunohistochemistry techniques (see below).

Cell cultures

EndoC-βH1/3 cell cultures and subcultures were maintained according to manufacturer's instructions, as previously described.[24,69] For the viability assays, EndoC-βH3 cultures were treated with 1 μM tamoxifen (Sigma) for 21 days, followed by 14 days of wash-out. Before treatments, EndoC-βH1/3 cells were starved ON in complete growth media supplemented with 2.8 mM glucose, while stimulations were performed using complete growth media supplemented with 2.8 mM glucose and 0.1% BSA.

Zebrafish studies

To ablate the β-cells, we incubated the double transgenic zebrafish larvae in E3 medium supplemented with 10 mM metronidazole (Sigma-Aldrich), 1% DMSO (VWR), and 0.2 mM 1-phenyl-2-thiourea (Acros Organics) from 3 to 4 dpf, as previously described.[70] During regeneration, the zebrafish larvae with ablated β-cells were treated with DMSO, sivelestat or telaprevir (Selleckchem) at

the concentrations indicated in the figures or figure legends from 4 to 6 dpf. The zebrafish larvae were then euthanized, fixed, immunostained, imaged and analyzed as previously described[62] with the anti-insulin primary antibody (1:100, Cambridge Research Biochemicals, customized).

Human pancreatic histological analysis

To evaluate the expression patterns of CELA3A and N-CELA3B (cleaved form) within the islet microstructure with respect to the insulin and E-cadherin immunostaining, confocal scans at 20X magnification was performed using a ScanScope (Aperio). Whole-pancreas scans were analyzed using the QuPath software.[68] Briefly, DAPI staining, marking the nuclei, was used to identify cells and E-Cadherin was used to mark cell borders. Then, cell segmentation was used to calculate cell-specific parameters, including cell area and N-CELA3B and insulin labeling intensity. Analysis of the exocrine N-CELA3B expression was conducted by measuring the intensity of N-CELA3B staining in INS^- cells across the whole pancreatic section, following normalization on the respective cell area, whereas the islet-specific N-CELA3B expression was assessed by quantifying the intensity of the signal in all the islets (marked by INS^+ staining, $\geq$40 islet per pancreatic section), following normalization on the islet area. The latter analysis was performed also in different lobules of the pancreatic sections, defined according to previously reported criteria.[71]

Mouse studies

For the dietary studies, 4-week-old male C57BL6/J mice were purchased from Jackson Labs and maintained on a low-fat diet (LFD, Research Diet, catalog# D12450J) or a high-fat diet (HFD, Research Diet, catalog# D12492) for 24 weeks. After a 20-week feeding with LFD or HFD, either vehicle (DMSO) or telaprevir at 30 or 300 μg/kg/day were administered for 28 days using osmotic pumps (Alzet) implanted subcutaneously in weight-matched animals, as previously described.[14] At the end of the follow-up period, mice were sacrificed, and pancreases were dissected, fixed, paraffin-embedded and sectioned. β-cell proliferation and mass were assessed using immunofluorescence techniques as described below. Metabolic assays, such as glucose tolerance test (GTT), insulin tolerance test (ITT) and *in vivo* glucose-stimulated insulin secretion (GSIS), were conducted on mice before pump implantations (week 0) and 4 weeks after treatments (week 4), using standard protocols.[69] Mouse insulin levels were measured by ELISA (CrystalChem) according to the manufacturer's instructions. For the human islet transplantation studies, 8-to-12-week-old male NSG mice were used. GTT, ITT and *in vivo* GSIS were performed at weeks 0 and 4 as earlier described. Serum human C-peptide levels were measured by ELISA (Mercodia) according to the manufacturer's protocol.

Quantification of CELA3B levels in human islets

We estimated the concentration of CELA3B in human islet samples from ND and T2D donors interpolating the amount of the CELA3B detected in islets using an anti-CELA3B antibody on a CELA3B standard curve, built by loading known amounts of PE by Western Blotting (see below). Then, we normalized the abundance of CELA3B to the initial concentration of the human islet lysates to derive the concentration of CELA3B in the total islet protein extracts. Knowing that lysates were extracted from 50 IEQs, which approximately contained 25,000 β-cells (considering an average of 1000 cells per IEQ,[72] and a 50% proportion of β-cells per islet[73]), we related the amount of CELA3B to $1x10^6$ β-cells and estimated a content of 312.3 ± 170.6 ng and 2183.7 ± 353.5 ng of CELA3B in ND and T2D islets, respectively. Since all the following experiments employing human β-cell lines were performed using $1x10^6$ cells/condition cultured in a 2 ml volume, we used a ~150 ng/ml and a ~1000 ng/ml concentration for mimicking the conditions observed in ND and T2D islet, respectively.

Human β-cell and islet cell treatments

EndoC-βH1/3 cells at low passage numbers (at $5.2x10^4$ cells/cm^2 density) or human islet cells were stimulated with 1X DPBS or human pancreatic elastase (PE, Elastin Product Company) in combination with either DMSO, or telaprevir (Selleckchem), and/or PAR2 inactivating peptide (FSLLRY-NH_2, Tocris).

RNA interference

Transient knock-downs in EndoC-βH1/3 were performed by combining the ON-TARGETplus Human PTK2 siRNA pool L-003164-00-0010 (Dharmacon) or the ON-TARGETplus Non-targeting siRNA pool D-001810-10-20 (Dharmacon) at 10 nM final concentration, with lipofectamine RNAiMAX (Invitrogen) according to manufacturer's instructions, as previously described.[69]

DNA plasmids

To induce overexpression of FAK, we transfected EndoC-βH1 cells with either an empty vector (EX-NEG-M35-B, Genecopoeia) or a construct containing the cDNA of PTK2 (NM_153831.3, EX-I0314-M35-B, Genecopoeia), both containing a 3X FLAG tag at the C-term, using lipofectamine 3000 (Invitrogen) according to manufacturer's instructions.

Viability assays in human β-cell lines

Following stimulations, EndoC-βH3 cells were trypsinized and incubated with EdU (5 μM) for 3 h at 37° C and 5% CO_2 using the Click-iT EdU Alexa Fluor 488 Flow Cytometry Assay Kit (Thermo Fisher) according to manufacturer's instructions. In parallel, β-cell apoptosis was examined by using the Annexin V labeling using the Dead Cell Apoptosis Kit (Thermo Fisher) following the manufacturer's instructions. At the termination of the staining, we counted up to 10,000 cells by flow cytometry using an LSRFortessa flow

cytometer (BD Biosciences). Data were analyzed with the FlowJo software (FlowJo LLC). Caspase 3 activity was measured using the Caspase-3/CPP32 Colorimetric Assay Kit (BioVision) according to manufacturer's indications. Absorbance variations were measured at 405 nm using a GloMax (Promega) plate reader.

Viability assays in human islet cells

Upon receipt, human islets were dispersed into single-cell preparations using TrypLE Express (Gibco) for 30 min at 37° C. Following neutralization of the dissociation agent using solutions with fetal bovine serum (FBS) and washings, islet cells were counted and seeded in ECM/fibronectin-coated plates. After ON incubation, cells were pre-treated with either RNAase-free sterile water (H_2O) or FSLLRY-NH_2 in stimulation media supplemented with EdU (10 μM). After 24 h, cells were incubated with stimulation media supplemented with vehicles or compounds, and EdU (10 μM). Following 24 h, cells were trypsinized and incubated with diacetylated Zinpyr1 (DA-ZP1), a fluorescent Zn-binding cargo which selectively labels human β-cells, using reported protocols.[36] Proliferative cells were stained using the Click-iT EdU Alexa Fluor 647 Flow Cytometry Assay Kit (Thermo Fisher), whereas the APC Annexin V reagent (BD) was used to label apoptotic cells, according to manufacturer's protocols. A minimum of 4000 live cells, negatively selected using Zombie NIR (New England Biolegend) labeling, were counted using a LSRFortessa flow cytometer (BD Biosciences). Data were analyzed with the FlowJo software (FlowJo LLC).

Immunofluorescence

Human pancreas and islet sections were incubated with the following primary antibodies: Ki67 (550609, BD), pHH3 (06-570, Millipore), CELA3A (sc-100527, Santa Cruz), N-term-CELA3B (N-CELA3B, SAB1306246, Sigma), E-Cadherin (14472, Cell Signaling), insulin (ab7842, Abcam), and glucagon (ab92517, abcam). Specific signal was detected by using fluorescence-conjugated anti-guinea pig, anti-rabbit and anti-mouse secondary antibodies (Alexa Fluor 488, Alexa Fluor 594, and AMCA, Jackson Immunoresearch). Images were captured using a Zeiss Axio Imager A2 upright fluorescence microscope or a Zeiss LSM-710 Confocal Microscope. The rodent β-cell mass was calculated by generating the ratio of the cross-sectional area of the total number of pixels of insulin-positive cells (from >50 islets per pancreatic section) to the cross-sectional area of the total number of pixels of the pancreatic tissue (using 2-3 pancreatic sections 200 μm apart per mouse), multiplied by the wet weight of the mouse pancreas. We evaluated β-cell proliferation in murine pancreas, and cultured/transplanted human islets by co-immunostaining sample sections with either Ki67 or pHH3 with insulin and DAPI (4,6-diamidino-2-phenylindole), as previously reported.[14] Cell death was detected using the non-radioactive terminal deoxynucleotidyltransferase-mediated deoxyuridine triphosphate nick end-labeling (TUNEL) reagent (ApopTag S7100, Chemicon) as previously described.[6]

Compound Libraries

The compound collections used in the High-Throughput Screening (HTS) assay included DMSO-dissolved small molecules (20 μM) from three different libraries, Performer, Informer and Repurposing set (Broad Institute). The Performer set consists of 2,240 compounds that have been selected based on their performance diversity across a wide set of cellular features, including gene expression and cell morphology.[29] The Informer set collection consists of 9,920 compounds synthesized by diversity-oriented synthesis (DOS)[26,28] and was assembled to maximally represent the diversity across all ~100,000 DOS compounds. The Repurposing Library is a well-annotated collection of more than 4500 compounds at different stages of clinical or preclinical development.[27]

High Throughput Screening

The assay used in the HTS was based on porcine pancreatic elastase activity and performed in black optical 384-well microplates (Corning Life Science), using the EnzCheck® Elastase Assay Kit (Thermo Fisher) according to the manufacturer's instructions. Briefly, each assay plate was prepared by aliquoting 25 μl/well of a porcine pancreatic elastase (pPE) solution (0.4 U/ml). Experimental compounds or sivelestat (positive control) were combined with the pPE solution at a concentration of 20 μM, using a CyBi-Well pin-transfer robot (CyBio Corp.). DMSO was used as a negative control. After incubation at RT for one hour, a solution containing elastin labeled with the BODIPY®FL dye (12.5 μg/ml), was added to the whole plate. The fluorescence released from the digestion of elastin by the protease was measured after 2 h incubation at RT using an Envision™ multimode plate reader (PerkinElmer), using 485/535 Ex/Em filters.

Statistical Analysis of HTS

DMSO, sivelestat and single compounds were tested at 20 μM in duplicates and the z-scores were calculated after normalizing the raw data on the DMSO values. Percentage of inhibition (%) was calculated by subtracting the blank to each value and normalizing it to the DMSO (as 0% of inhibition) and to sivelestat (as 100% of inhibition) values. A percentage of inhibition value of 50% for each replicate was considered as a cut-off for hits identification to reach a significant area of ≥3 standard deviations from the mean of the DMSO values. IC_{50} values were calculated using the GraphPad Prism® software program (v9.3, La Jolla, CA) as previously reported.[74]

Static glucose-stimulated insulin secretion assays

EndoC-βH1 cells were incubated in 2.8 mM glucose containing DMEM growth media supplemented with either vehicles (PBS and DMSO) or PE (500 ng/ml) and telaprevir (1.5 μM) alone or in combination. After overnight starvation, media was replaced with fresh

Krebs Ringer Buffer (KRB) containing NaCl (115 mM), NaHCO3 (24 mM), KCl (5 mM), MgCl2 (1 mM), CaCl2 (1 mM), HEPES (10 mM), BSA (0.2% wt/vol), 2.8 mM glucose for 1 hr. Static insulin secretion assays were then initiated by adding KRB containing 2.8 mM or 11.1 mM glucose and PE +/- telaprevir for 1 hr. Aliquots of supernatants were removed, centrifuged to discard dead cells and stored for analysis in ice-cold acid ethanol that was added to extract DNA content from cells following sonication. Insulin secretion and was measured by the human insulin ELISA (Mercodia, USA) according to the manufacturer's instructions. DNA amounts were measured using Nanodrop 1000 spectrophotometer.

Perifusion experiments

EndoC-βH1 pseudoislets were generated by seeding cells into a fresh plate coated with 1% gelatin. Cells were allowed to aggregate for 2 days and were then divided into two gelatin-coated 6 cm plates. Porcine pancreatic elastase (PE, 500 ng/ml) or vehicle control (PBS, 0.05 % v/v) was then added, and the cells treated overnight. Treated pseudoislets were loaded into Biorep perifusion chambers mixed with Biogel P4 beads. These chambers (3 each for control and PE) were then mounted into the Biorep perifusion system. Once the system reached 37°C, perifusion was started at a rate of 100 μl/min. The base perifusion solution contained (in mM): 120 NaCl, 4.8 KCl, 2.5 CaCl2, 1.2 MgCl2, 10 HEPES, 24 NaHCO3 and 0.1% BSA (pH adjusted to 7.4). Concentrations of glucose as indicated were added along with vehicle or pPE. A perifusion equilibration period of 32 min was followed by sample collection in 96 well plates as indicated. After completion of the perifusion protocol, cell aggregates were recovered from the chambers and lysed in 0.5 ml of acid-ethanol for measurement of total insulin after dilution 1:100 in buffer. Insulin in both perifusate and total insulin samples was measured using Mercodia Human insulin ELISA kits (Cat. # 10-1113-01) and calibrated using the solutions provided. ELISA plate optical densities were measured at 450 nm using a Bio Rad Benchmark Plus plate reader and converted to insulin concentrations using Bio Rad Microplate Manager software. Data was exported into Origin 2018.2 software for plotting.

Single-cell RNA-Sequencing

Human islet samples were treated with either DMSO or compounds for single-cell RNA-sequencing (scRNA-Seq) using the Chromium single-cell 3' Library Kit (10X Genomics). Briefly, after treatment modalities were performed as described above, we dispersed human islets using Accutase (Gibco) for 20 minutes at 37°C, to obtain single-cell preparations. Dead cells were sorted using the Dead Cell Removal Kit (Miltenyi Biotec), following the manufacturer's instructions. After cell counting and confirming cell viability $\geq$80%, we encapsulated 10,000 cells into barcoded Gel Beads in Emulsion (GEMs) and the cDNA amplification and library construction reactions were performed according to the manufacturer's protocol. The final single-cell libraries were sequenced using a coverage of 500,000 pair-ended reads targeted per cell, on a HiSeq platform (Illumina) by GeneWiz laboratories (NJ, USA).

Analysis of scRNA-Seq datasets

Quality controls of scRNA-Seq outputs (GSE190447), including library sizes, number of expressed genes and proportion of unique molecular identifiers (UMIs) assigned to mitochondrial genes, were computed using the R package Scater[75] to remove low-quality cells with a small library size, non-barcoded reads and cells with a proportion of mitochondrial genes >20%. Low-abundant genes with average counts <0.01 were also excluded. Cells were clustered using the deconvolution method[76] and cell types were classified according to the expression of glucagon (*GCG*, α-cells), insulin (*INS*, β-cells), somatostatin (*SST*, δ-cells), pancreatic polypeptide (*PPY*, PP-cells), ghrelin (*GHRL*, ε-cells), serine protease 1 (*PRSS1*, acinar cells), cytokeratin 19 (*KRT19*, ductal cells), collagen type I α1 chain (*COL1A1*, mesenchymal cells), and endothelial cell adhesion molecule (*ESAM*, endothelial cells) as previously described.[77] To discover the differential expressed genes, we used edgeR package following empirical Bayes quasi-likelihood F-tests for comparisons in the several cell types.[67] For these initial analyses we focused on the differential expressed genes with a false discovery rate (FDR) <0.05 and a fold change (FC) $\gtrless$|1.2| in comparison to the control samples. Canonical pathway analysis was performed within the β-cell dataset, considering the selected genes. Directionality of pathway regulation was determined using Fry function of the Rotation Gene Set Test (Roast) in the limma R package.[78] An FDR<0.05 was used to select significantly regulated pathways.

Phospho-antibody microarray

The phospho-antibody microarray studies were performed on treated human islets using the Kinexus Antibody Microarray (KAM 1325, Kinexus), consisting of 875 phosphosite-specific antibodies for detecting phosphorylations, and 450 pan-specific antibodies for measuring total protein levels, according to the manufacturer's protocols.[69]

Analysis of phopsho-antibody microarray datasets

The phospho-antibody microarray outputs (GSE189986) were initially analyzed by normalizing the background-corrected raw intensity data to the overall average of the signals released by a single slide, to obtain z-score values, as previously described.[79] Then, the phosphosite data were normalized to those of the respective total proteins. For analyzing the differentially regulated phosphosites (DRPs), we used limma, an R package that powers differential expression analyses.[66] Canonical pathway analysis was performed using the publicly available resource ConsensusPathDB (http://cpdb.molgen.mpg.de) as previously reported,[69] selecting phosphosites whose levels significantly changed in human islets treated either with telaprevir or sivelestat compared to controls with an FC $\gtrless$|1.2| (*P* value<0.05).

Please cite this article in press as: Basile et al., Excess pancreatic elastase alters acinar-β cell communication by impairing the mechano-signaling and the PAR2 pathways, Cell Metabolism (2023), https://doi.org/10.1016/j.cmet.2023.05.007

Transcription factor analysis

To integrate the phospho-antibody microarray and scRNA-seq outputs we first selected transcription factor proteins (TFs) among the significantly differentially phosphorylated proteins in telaprevir vs. DMSO at both 10 and 30 mins. By using the publicly available resource Molecular Signatures Database (MsigDB),[80,81] we identified the gene sets as targets of the selected TFs, among the significantly differentially regulated genes in telaprevir vs. DMSO β-cells. ConsensusPathDB was used for pathway analysis, using the enriched gene sets per TF as input.

Brillouin imaging

To assess the mechanical state of human β-cells following exposure to PE and its inhibition we treated EndoC-βH1 cells with either vehicles, PE at 250 ng/ml or PE + telaprevir (at 750 nm). After 24 hr incubation, we measured the stiffness of 12 cells/conditions using Brillouin Microscopy. Brillouin microscopy enables non-contact, spatially resolved mapping of the longitudinal mechanical properties of tissues.[82] Brillouin data were obtained using a confocal Brillouin microscope with a 780 nm single-frequency laser and a virtually imaged phase array (VIPA) spectrometer, which has been described previously.[83,84] This instrument measures the GHz-scale frequency shift of inelastically backscattered light from naturally occurring compressional waves in tissue (spontaneous Brillouin scattering). The Brillouin frequency shift measured is proportional to the propagation speed of compressional waves which is a function of the local longitudinal modulus in tissue. The Brillouin measurement volume per point was approximately 0.5 x 0.5 x 1.0 μm and the integration time per point was 200 ms. For each EndoC-βH1 cell, a co-aligned brightfield microscope was used to navigate to the mid-plane of the cell vertically and a 2D scan spanning the central cross-section and surrounding medium was acquired covering an area of approximately 20 x 20 μm (40 x 40 points). Because the cell has a significantly higher Brillouin value (∼5.30 GHz) compared to the surrounding medium (∼5.05 GHz), the perimeter of the cell could be delineated using a simple threshold set by Li's iterative Minimum Cross Entropy method.[85] This permitted averaging of the Brillouin frequency shift across all points within the cross-section, yielding a single Brillouin value for the cell.

Western Blotting

Total proteins were collected from lysates prepared from human islets, human acinar cells and β-cell line samples using RIPA protein extraction reagent (Thermo Fisher) supplemented with proteinase and phosphatase inhibitors (Sigma), according to manufacturer's protocols. Protein concentrations were determined using the BCA method followed by standard western immunoblotting of proteins using different primary antibodies: anti-CELA3A (sc-100527, Santa Cruz), anti-CELA3B (CELA3B, SAB1409028, Sigma), anti-N-termCELA3B (N-CELA3B, SAB1306246, Sigma), anti-Trypsin (sc-137077, Santa Cruz), anti-Amylase (sc-46657, Santa Cruz), anti-PDX1 (5679, Cell Signaling), anti-PAR2 (35-2300, Thermo Fisher), anti-PAR3 (sc-393127, Santa Cruz), anti-FAK (3285, Cell Signaling), anti-PAK1^{S144} (2606, Cell Signaling), anti-PAK1 (2604, Cell Signaling), anti-ERK1/2$^{T202+Y204}$ (9101, Cell Signaling), anti-ERK1/2 (9102, Cell Signaling), anti-β-Actin (4970, Cell Signaling), anti-Vinculin (sc-73614, Santa Cruz), and anti-GAPDH (5174, Cell Signaling). To evaluate the affinity of the anti-CELA3B and anti-N-CELA3B antibodies we used a recombinant protein corresponding to the cleaved form (aa 29-270) of the human CELA3B protein (MBS2012053, MyBioSource). The blots were developed using chemiluminescent substrate ECL (Thermo Fisher) and quantified using ImageJ.

RNA isolation and RT-PCR

High-quality total RNA (>200 nucleotides) was extracted from ND and T2D human islet, ductal cells and acinar cell samples using standard TRIzol reagent according to the manufacturer's instructions, and the resultant aqueous phase was mixed (1:1) with 70% RNA-free ethanol and added to Qiagen RNeasy mini kit columns following the manufacturer's protocols. The quality and quantity of the isolated RNA were evaluated using a NanoDrop One Spectrophotometer (Thermo Fisher). cDNA was produced by reverse transcription using the high-capacity cDNA synthesis kit (Applied Biosciences). Human bone marrow cDNA (Takara) was used as neutrophil protease source. Gene amplification was performed by using specific oligonucleotides as primers (sequences in Table S2) and monitoring SYBR green incorporation in cDNAs through real time polymerase reaction chain (RT-PCR) using the ABI 7900HT system (Applied Biosciences). Gene expression was calculated using the ΔΔCt method following normalization on *ACTB* levels.

Absorbance-based protease activity assay

The protease-activity assay was performed in 96-well ELISA assay plates (Corning Life Science) according to previous publications.[14] Briefly, 500 ng of human pancreatic elastase (PE), porcine pancreatic elastase (pPE), human neutrophil elastase (NE) or human cathepsin G (cat G) (Elastin Products Company), were combined with 15 two-fold dilutions of sivelestat (Selleckchem), telaprevir (Selleckchem) or tebipenem (SigmaAldrich), starting from the compound concentration used in the HTS assay (20 μM). Wells without enzymes (blank) and wells with enzymes and DMSO (DMSO) were added to the plates as internal experimental controls. Plates were incubated for 3 minutes at 37°C and the substrates were added. N-Methoxysuccynil-Ala-Ala-Pro-Val-*p*-nitroanilide (Calbiochem) was used as substrate for the PE, pPE, and hNE, while the Succinyl-Ala-Ala-Pro-Phe-*p*-nitroanilide (Elastin Product Company) was the substrate for the cat G activity assays. The changes in absorbance of NE and cat G reactions were immediately measured, while pPE and human PE reactions were measured after 2 h incubation with their respective substrate at 37°C, reading the assay plates at 405 nM at 15 seconds for 21 reads (5 minutes in total) using a GloMax plate reader (Promega).

Please cite this article in press as: Basile et al., Excess pancreatic elastase alters acinar-β cell communication by impairing the mechano-signaling and the PAR2 pathways, Cell Metabolism (2023), https://doi.org/10.1016/j.cmet.2023.05.007

QUANTIFICATION AND STATISTICAL ANALYSIS

Sample size in our *in vitro* or *in vivo* studies were determined according to our experience from previous works. For analyzing significance between two groups, we used two-tailed unpaired or paired t-test. For determining significance among more than two groups we used unpaired or paired One-Way ANOVA test or Two-Way ANOVA test with multiple comparisons adjustments as indicated in the figure legends. Association between the amount of N-CELA3B measured in the exocrine and endocrine compartments was tested by performing Pearson's linear correlation. Statistical tests were performed using GraphPad Prism software program (v9.3, La Jolla, CA). A P value<0.05 was considered significant.